AD-A193 706 LASER AND ELECTROCHEMICAL STUDIES OF METALLIZATIONS IN ELECTRONIC DEVICES(U) ISRAEL INST OF METALS HAIFA J ZAHAVI ET AL. DEC 87 EOARD-TR-88-03 AFOSR-86-0315 1/1

UNCLASSIFIED F/G 9/3 NL

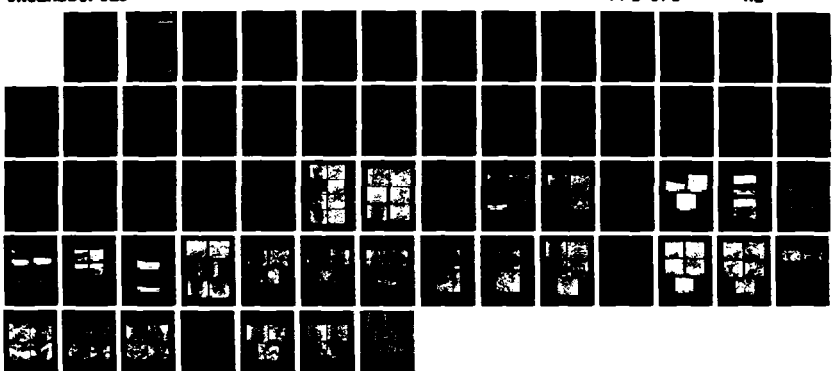

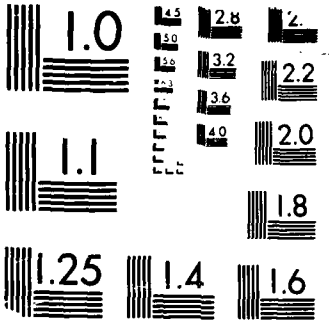

MICROCOPY RESOLUTION TEST CHART

MINISTRY OF INDUSTRY & TRADE
INDUSTRIAL R & D ADMINISTRATION
משרד התעשיה והמסחר
המינהל למחקר ופיתוח תעשיתי

ISRAEL INSTITUTE OF METALS · מכון המתכות הישראלי

TECHNION RESEARCH AND DEVELOPMENT FOUNDATION LTD.
מוסד הטכניון למחקר ופיתוח בע"מ

LASER AND ELECTROCHEMICAL STUDIES OF METALLIZATIONS IN ELECTRONIC DEVICES

Second Annual Research Report
No. 504-591

1 Sep 86 - 31 Aug 87

J. Zahavi
M. Rotel

Israel Institute of Metals

B. Dobbs

WPAFB, MLSA, Dayton, Ohio 45433, U.S.A.

Technion City, Haifa, December 1987

UNCLASSIFIED
SECURITY CLASSIFICATION OF THIS PAGE

AD-A193 756

REPORT DOCUMENTATION PAGE

1a. REPORT SECURITY CLASSIFICATION: Unclassified	1b. RESTRICTIVE MARKINGS
2a. SECURITY CLASSIFICATION AUTHORITY	3. DISTRIBUTION/AVAILABILITY OF REPORT: Approved for public release; Distribution unlimited
2b. DECLASSIFICATION/DOWNGRADING SCHEDULE	
4. PERFORMING ORGANIZATION REPORT NUMBER(S)	5. MONITORING ORGANIZATION REPORT NUMBER(S): EOARD TR-88-03
6a. NAME OF PERFORMING ORGANIZATION: Israel Institute of Metals; 6b. OFFICE SYMBOL (If applicable)	7a. NAME OF MONITORING ORGANIZATION: European Office of Aerospace Research and Development
6c. ADDRESS (City, State, and ZIP Code): Technion - Israel Institute of Technology, Technion City, Haifa 32 000, Israel	7b. ADDRESS (City, State, and ZIP Code): Box 14, FPO New York 09510-0200
8a. NAME OF FUNDING/SPONSORING ORGANIZATION: AFWAL Materials Laboratory and EOARD; 8b. OFFICE SYMBOL (If applicable): MLSA/LRP	9. PROCUREMENT INSTRUMENT IDENTIFICATION NUMBER: AFOSR 86-0315
8c. ADDRESS (City, State, and ZIP Code): AFWAL/MLSA, Wright-Patterson AFB, OH 45433-6533; EOARD/LRP, Box 14, FPO New York 09510	10. SOURCE OF FUNDING NUMBERS: PROGRAM ELEMENT NO. 61101F/61102F; PROJECT NO. 2301; TASK NO. D1; WORK UNIT ACCESSION NO. 025
11. TITLE (Include Security Classification): LASER AND ELECTROCHEMICAL STUDIES OF METALLIZATIONS IN ELECTRONIC DEVICES	
12. PERSONAL AUTHOR(S): J. Zahavi and M. Rotel	
13a. TYPE OF REPORT: Interim Scientific; 13b. TIME COVERED: FROM 1 Sep 86 TO 31 Aug87; 14. DATE OF REPORT (Year, Month, Day): 1987 December; 15. PAGE COUNT	
16. SUPPLEMENTARY NOTATION	
17. COSATI CODES: FIELD / GROUP / SUB-GROUP	18. SUBJECT TERMS (Continue on reverse if necessary and identify by block number): Laser treatment, Pb-Sn coating, corrosion, potentiodynamic polarization.

19. ABSTRACT (Continue on reverse if necessary and identify by block number)

The research during this year was concerned with application of excimer laser (193nm, 24 nsec, 10^6-10^7 watt/cm^2 pulse) to Pb-Sn surfaces. The laser induced melting of the Pb-Sn coating resulted in bright area in which lead-rich zone were observed. Perferential dissolution of lead was observed during electrochemical potentiodynamic polarization of both the as-deposited and laser treated surfaces. Calculation showed that the laser-treated specimen had higher corrosion rates than as-deposited counterparts.

20. DISTRIBUTION/AVAILABILITY OF ABSTRACT: ☑ UNCLASSIFIED/UNLIMITED ☐ SAME AS RPT. ☒ DTIC USERS	21. ABSTRACT SECURITY CLASSIFICATION: Unclassified
22a. NAME OF RESPONSIBLE INDIVIDUAL: LARELL K. SMITH, Lt Col, USAF	22b. TELEPHONE (Include Area Code): (44 1) 409-4505; 22c. OFFICE SYMBOL: EOARD/LRP

DD FORM 1473, 84 MAR — 83 APR edition may be used until exhausted. All other editions are obsolete.

SECURITY CLASSIFICATION OF THIS PAGE
UNCLASSIFIED

EOARD-TR-88-03

This report has been reviewed by the EOARD Information Office and is releasable to the National Technical Information Service (NTIS). At NTIS it will be releasable to the general public, including foreign nations.

This technical report has been reviewed and is approved for publication.

LARELL K. SMITH, Lt Col, USAF
Chief, Physical Chemistry/Materials

PHILIP J. CONRAN, Colonel, USAF
Commander

Technion Research
and Development Foundation

Israel Institute
of Metals

LASER AND ELECTROCHEMICAL STUDIES OF METALLIZATIONS IN ELECTRONIC DEVICES

Second Annual Research Report
No. 504-591
1 Sep 86 - 31 Aug 87

J. Zahavi
M. Rotel

Israel Institute of Metals

B. Dobbs

WPAFB, MLSA, Dayton, Ohio 45433, U.S.A.

Technion City, Haifa, December 1987

CONTENT

1. INTRODUCTION

The research during this year was concerned with application of excimer laser to Pb-Sn surfaces as a means of thermal treatment of the coated area.

In this year the laser was used to produce large surfaces in order to study the effect of laser treatment on corrosion resistance of the Pb-Sn surfaces.

The treated and untreated surfaces were compared in terms of electrochemical potentiodynamic polarization.

The corroded area morphology shows that the corrosion proceeds primarily though preferential lead (Pb) dissolution.

The laser-treated surfaces had higher corrosion rates than the as-deposited specimens.

The laser treatment may have produced a melted surface of the Pb-Sn and of the Sn coatings, similar to surfaces observed after the reflow process as noted in the previous annual report.

2. EXPERIMENTAL

2.1 Laser Operation

The laser used in our experiment this year was excimer laser manufactured by Lambda Physics Model 201MSC working at 193nm with pulse duration of 24nsec. The activated laser material is a mixture of Ar and F_2 gases in which produces activated molecules of ArF. The beam mode was rectangular with a small hole in the center. The beam dimensions were

0.8x2cm, and it was directed perpendicular to the specimen surface by a 45° turning mirror after passing through an aperture that cut the beam in half in order to eliminate the hole in the center of the beam cross-section (Fig. 2.1). Prior to irradiation, the beam cross-section area was measured and the energy per pulse for this section was monitored by power meter.

Specimen movements were controlled by a computerized x-y table. The specimen was shifted during the treatment so as to produce overlapping between the adjusted pulses.

Laser energy per pulse was calculated according to the formula:

$$watt/cm^2 = W/R.R \cdot A \cdot t_p$$

where

W - energy measured by heat-sensitive apparatus (watt)
R.R - repetition rate pulses per second
A - area of laser beam cross-section (cm^2)
t_p - duration of laser pulse (24nsec in our experiment)

The laser beam power ranged from about 0.4 to 1 Watt at 10 pulses per sec, while the beam cross-section area was $0.2cm^2$ to $0.5cm^2$. Accordingly, the energy per pulse was $8 \cdot 10^6 watt/cm^2$.

2.1.1 Laser Conditions

The laser energy applied was calculated from the energy per pulse and the overlapping between the pulses. Table 2.1 summarizes the laser conditions applied.

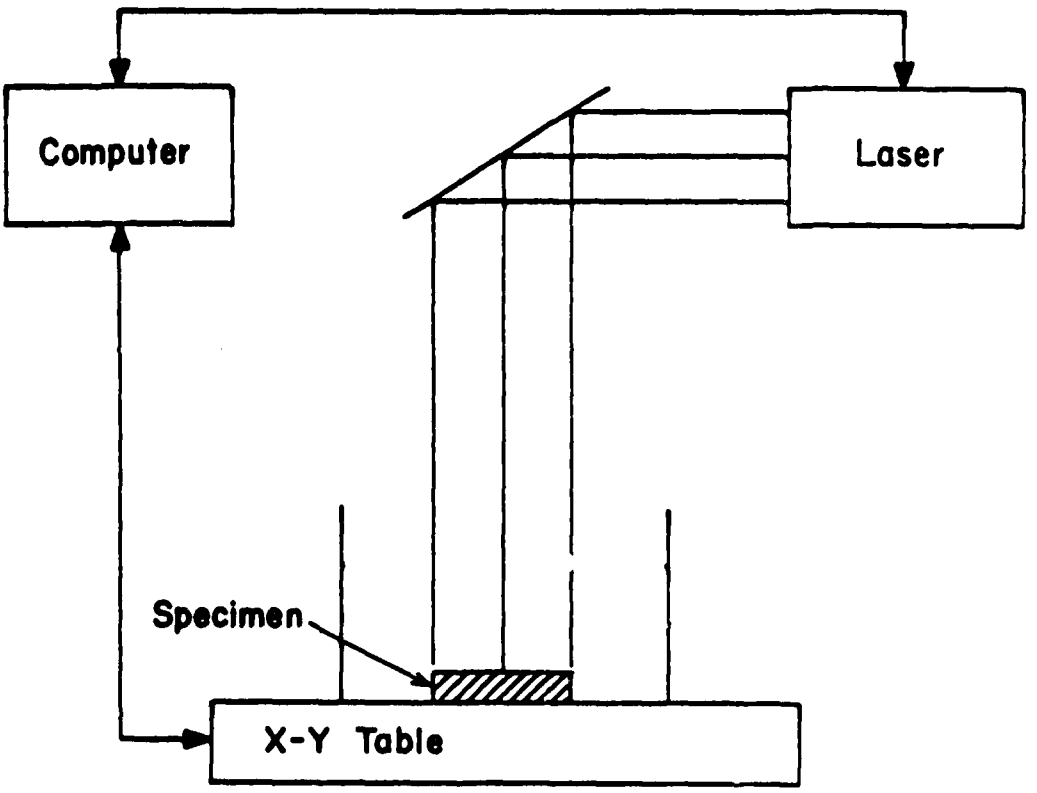

Fig. 2.1: Schematic set-up

Table 2.1: Laser energy conditions

Exp. Table No.	Sample No.	Energy per Pulse [Watt]	R.R [Pulse/sec]	Over-lapping	No. of Pulses per Area	Energy Density [Watt/cm^2]
3.1	all	$2.9X10^6$	10	50%	10	$5.9X10^7$
3.2	all	$3X10^6$	10	50%	10	$6X10^7$
3.3	1	$2.5X10^6$	10	50%	10	$5X10^7$
	2	$1.5X10^6$	10	50%	10	$3X10^7$
	3	$1.5X10^6$	10	50%	10	$3X10^7$
	4	$1.9X10^6$	10	50%	10	$3.8X10^7$
3.4	all	$3X10^6$	10	50%	10	$6X10^7$

2.2 Polarization

Potentiodynamic polarization was carried out in 10^{-2}M NaCl solution. The resulting polarization curves provided information regarding the corrosion behavior of the Pb-Sn coating in aqueous solution. Corrosion rates were calculated in millinch per year (MPY) units.

The polarization curves were obtained with the aid of a corrosion measurement system model 350A manufactured by Princeton Applied Research. The detailed set-up of the experiments was given in the previous report.

Polarization parameters were:
Scan rate: 0.5mv/sec
Initial potential: -1.0 Volt (versus S.C.E.)
Vertex potential: 0.0 Volt (versus S.C.E.)
Final potential: -1.0 Volt (versus S.C.E.)
Initial delay: 5 minutes

These parameters were used in all the experiments with a view to satisfactory comparability.

2.3 Specimen

The polarized specimen types were:

A: As deposited laboratory prepared Pb-Sn coatings on copper foil with varing coating thickness.

B: Laser treated laboratory Pb-Sn coatings on copper foil with varing coating thickness.

C: Commercial as deposited Pb-Sn coating on epoxy plated with 70µm electroless copper.

D: Laser treated commercial specimen.

E: As-deposited tin plated or copper foil.

F: Laser treated tin plated surfaces.

2.4 Electroplating

Tin-Lead Alloy Plating was described in detail in the previous report. The coating was plated from a fluoborate bath supplied by Galvanocor which was built up according to the following formula:

Lead fluoborate	- 41 gr/l
Tin fluoborate	-120 gr/l
Fluoboric acid	-140 gr/l
Boric acid	- 10 gr/l
Additive LA1	- 15 gr/l
Additive LA2	- 15 gr/l
Stabilizer LA5	- 15 gr/l

The coating thickness was varied by changing the plating time.

Tin plating was done from tin fluoborate bath which was built up from

Stannous fluoborate	115 ml/l
Flouboric acid	380 ml/l
Boric acid	29.9 gr/l
LA1	15 ml/l
LA2	5 ml/l
LA3	11.5 ml/l

The coating thickness was varied by changing the plating time. The current density was 15mA/cm^2. Tin foil was used as anode.

3. RESULTS AND DISCUSSION

3.1 Potentiodynamic Polarization

Potentiodynamic polarization was carried out in order to assess the susceptibility of Pb-Sn alloy coating and tin coating to corrosion in chloride solution.

Corrosion rates of the various specimens in 10^{-2}M NaCl solution are shown in Tables 3.1-3.4, Typical potentiodynamic polarization curves are shown in Figs. 3.1-3.4.

According to the electrochemical theory of polarization (see previous report), the corrosion rates can be calculated by two methods: (A) the polarization resistance technique; (B) the Tafel technique.

According to method A a range of ±25mv around Ecorr is used for determination of the slope of the line (Fig. 3.4A).

$$(1) \quad \frac{\Delta E}{\Delta I} = R_p = \frac{\beta_A \cdot \beta_C}{2.3 I_{corr}(\beta_A+\beta_C)}$$

$$\text{or} \quad I_{corr} = \frac{\beta_A \cdot \beta_C}{2.3(\beta_A+\beta_C)} \cdot \frac{1}{R_p}$$

where

β_C - cathodic Tafel constant (volts)

β_A - anodic Tafel constant (volts)

I_{corr} - corrosion current density (A/cm²).

I_{corr} can be determined from the slope of the line by using equation (1). The calculated I_{corr} can be used to determine the corrosion rate according to equation (2), which was derived from Faraday's law.

(2) Corrosion rate (mpy)= $\frac{0.13 I_{corr} \cdot EW}{d}$

where

EW - equivalent weight (gr)
d - density of corroding species (gr/cm^3).
mpy - millinch per year

Fig. 3.4A shows an example of the curve obtained by the linear polarization technique and the straight line represents the calculated slope.

According to method B, the projection of the intersection of the Tafel constant with Ecorr determines I_{corr}, and this Icorr is used to calculate the corrosion rate by using equation (2). By this method, we can find I_{corr} from only one of the Tafel constants. This is of advantage where the Tafel constants differ widely. The cathodic Tafel constant is usually selected for I_{corr} determination because in the cathodic mode the specimen is free from oxidation products that can affect its behavior during polarization (Fig. 3.4B).

Tables 3.1-3.4 summarizes the calculations of the various polarization parameters by using the two methods described above. Icorr was calculated through the linear polarization method (R_p) while I_{corr}^c through the cathodic Tafel constant.

Figs. 3.5 and 3.6 show the correlations obtained by regression between I_{corr} and $1/R_p$ and between I_{corr}^c and $1/R_p$, respectively. I_{corr}^c was calculated the cathodic Tafel constant, as for many specimens the anodic Tafel constant was unobtainable.

The correlation found by using both Tafel constants (Fig. 3.5) through the linear polarization (R_p) method was:

(3) $I_{corr}=0.02 \cdot 10^{-6}+4.42 \cdot 10^{-2} \cdot 1/R_p$
$r=0.94$

where

I_{corr} in amp/cm²

R_p in Ωcm²

r - correlation coefficient

I_{corr} at $1/R_p=0$ is very small and can be neglected. We can assume that

$$\frac{\beta_A \cdot \beta_C}{2.3(\beta_A+\beta_C)} = 4.42 \cdot 10^{-2} \cdot \frac{1}{R_p}$$

The correlation found by using the cathodic Tafel constant was:

$$I_{corr}^{c} = 1.67 \cdot 10^{-6} + 1.7 \cdot 10^{-2} \cdot 1/R_p$$

$$r = 0.47$$

where

Icorr in amp/cm²

$1/R_p$ in $\Omega^{-1}cm^{-2}$

r - correlation coefficient

This second correlation was not very good and it seems that we cannot use it for corrosion behavior estimation. The difference between the cathodic and anodic Tafel constants rules out a linear relationship between $Icorr^c$ and $1/R_p$. (This difference may be a consequence of the corrosion type, which was found to be more local and intergranular than the general type).

The first correlation was used to calculate the corrosion current for specimens whose I_{corr} could not be calculated through both Tafel constants.

Tables 3.1÷3.3 indicate that for most of the specimens I_{corr} was higher for the laser treated specimens than for the untreated ones. For example, for coating thickness 12.7μm (Table 3.2) the I_{corr} found for the laser treated specimen was $1.046 \cdot 10^{-6}$amp/cm² and for as-deposited specimen $0.065 \cdot 10^{-6}$amp/cm². The calculated values obtained from the linear relationship were $1.37 \cdot 10^{-6}$ and

$0.05 \cdot 10^{-6}$amp/cm², respectively.

Similarly, for the commercial specimen (Table 3.3) the calculated I_{corr} of the untreated specimen was $0.92 \cdot 10^{-6}$amp/cm² and for the laser treated specimen $2.64 \cdot 10^{-6}$ and $1.21 \cdot 10^{-6}$amp/cm². Higher I_{corr} values resulted in higher corrosion rates in accordance with equation (2).

The same pattern was observed for the tin coating where the I_{corr} of the laser treated surface was $0.1036 \cdot 10^{3}$n/cm² as against $0.1533 \cdot 10^{3}$nA/cm² for the as-deposited specimen.

Figs. 3.1÷3.3 indicate that the polarization curves obtained were not the typical ones with equal anodic and cathodic Tafel constants, but the anodic curve shows a similarity to passivation behavior, i.e. potential increase without current increase. This behavior interferes with the corrosion rate calculations and can produce errors. The unfavorable correlation between Icorr^{e} and $1/R_p$ supports this explanation. The corrosion morphology observed by scanning electron microscope also supports this possibility.

Table 3.1: Corrosion rate calculations for Pb-Sn coatings on copper foil in 10^{-2}M NaCl before and after laser treatment

Specimen No.	Coating Thickness [μm]	Laser Treatment +/-	Icorr x10^3 [nA/cm^2]	Ecorr mv [S.C.E.]	Corrosion Rate [MPY]	Rp x10^4 [Ωcm^2]	Icorr^C x10^3 nA/cm [nA/cm^2]	Corrosion Rate [MPY^C]	Icorr Calculated x10^3 [nA/cm^2]
	(1)	(2)	(3)*	(4)	(5)*	(6)*	(7)**	(8)**	(9)***
53	1.89	+	0.1868	-607	0.040	15			0.295
54	1.96	-		-744		14.4			0.304
55	2.178	-	0.037	-500	0.008				
56	2.081	+		-464		0.57	2.606	2.994	1.73
62	4.3	-		-536		6.275			0.703
73	8.1	-	3.34	-654	0.720	2.43	0.9519	1.093	1.8
74	8.1	+	6.6	-409	1.416	0.7099	0.8301	0.954	6.2
87	12.6	-	1.248	-504	0.269	2.89	0.3608	0.414	1.5

* Calculated through linear polarization by the instrument

** Calculated through cathodic Tafel only by the instrument

*** Calculated by equation (3) p. 8.

Table 3.2: Corrosion rate calculations of Pb-Sn coatings in 10^{-2}M NaCl before and after laser treatment

Specimen No.	Coating Thickness [μm]	Laser Treatment +/-	Icorr x10^3 [nA/cm^2]	Ecorr mv [S.C.E.]	Corrosion Rate MPY	Rp x10^4 [Ωcm^2]	Icorr^c x10^3 [nA/cm^2]	Corrosion Rate [MPY]^c	Icorr Calculated x10^3 [nA/cm^2]
	(1)	(2)	(3)*	(4)	(5)*	(6)*	(7)**	(8)**	(9)***
24	2.7	+	5.075	-440	1.093	0.97	3.016	0.649	4.57
25	2.9	-		-527		2.96	0.323	0.371	1.486
64	4.3	-	1.515	-612	1.740	1.63	1.638	1.882	2.7
76	8.4	+	22.74	-388	26.1	0.348	9.657	11.09	12.6
75	8.4	-		-688		1.865	1.375	1.584	2.36
43	16.4	+	3.802	-437	4.367	1.35	5.114	5.874	3.25
42	15.6	-		-574	0.01	69.3	7.803	8.962	0.06
48	23.7	+	1.343	-418	1.543	2.08	3.807	4.373	2.115
83	12.7	+	1.046	-420	1.201	3.213	1.998	2.295	1.37
86	12.6	-	0.065	-652	0.075	80.40	0.069	0.794	0.05

* Calculated through linear polarization by the instrument

** Calculated through cathodic Tafel only by the instrument

*** Calculated by equation (3) p. 8.

Table 3.3: Corrosion rates of Pb-Sn commercial coating on electroless copper on epoxy in 10^{-2}M NaCl before and after laser treatment

Spec. No.	Coating thick-ness [μm]	Laser Treat-ment +/-	I_{corr}^{c} $x10^{3}$ [nA/cm^2]	Corro-sion Rates [MPY]	Ecorr mv [V.SCE]	Rp $x10^{4}$ [Ωcm^2]	I_{corr}^{c} Calcula-ted $x10^{3}$ [nA/cm^2]
	(1)	(2)	(3)**	(4)**	(5)	(6)*	(7)***
0	15	-	0.317	0.205	-0.526	4.75	0.92
1	15	+	2.59	1.676	-0.455	1.50	2.64
2	15	+	2.81	1.82	-0.482	3.63	1.21

* Calculated through linear polarization by the instrument

** Calculated through cathodic Tafel only by the instrument

*** Calculated by equation (3) p. 8.

Table 3.4: Corrosion rates of Sn coatings on copper foil in 10^{-2}M NaCl before and after laser treatment

Speci. No.	Coating Thick-ness μm	Laser Treat-ment +/-	Icorr $x10^{3}$ nA/cm^2	Ecorr mv V.S.C.E.	Corro-sion Rates MPY
2	0.9	+	2.054	-0.221	2.250
5	3.67	+	0.1036	-0.250	0.114
8	3.6	-	0.1533	-0.637	0.168

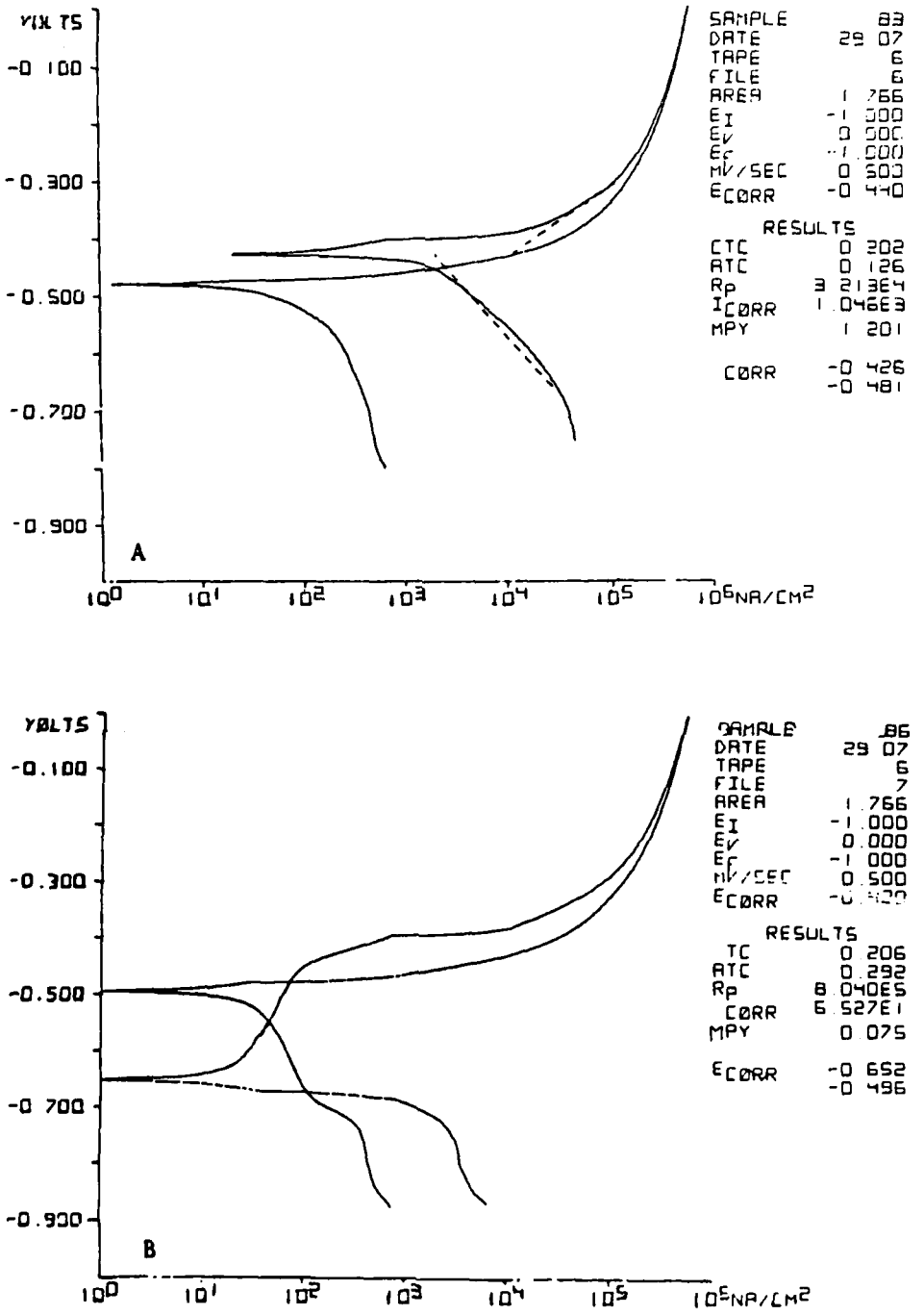

Fig. 3.1: Typical cyclic potentiodynamic curves obtained for Pb-Sn coatings in 10^{-2}M NaCl. (Coating thickness 12.6μm). A. After laser treatment. B. As-deposited specimen.

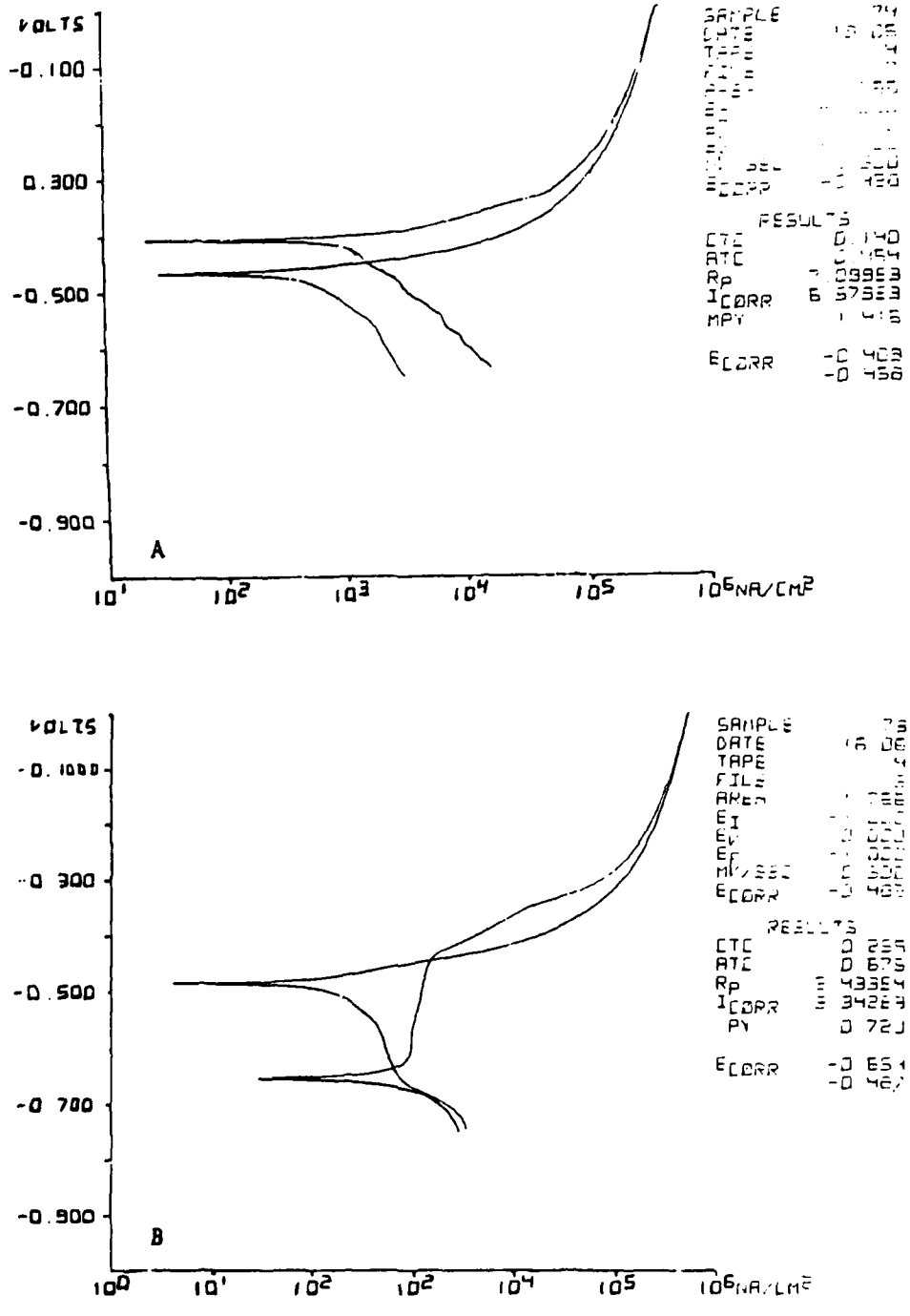

Fig. 3.2: Typical cyclic potentiodynamic polarization in 10^{-2}M NaCl of Pb-Sn coatings (coating thickness 8.1μm). A. After laser treatment. B. As-deposited specimen

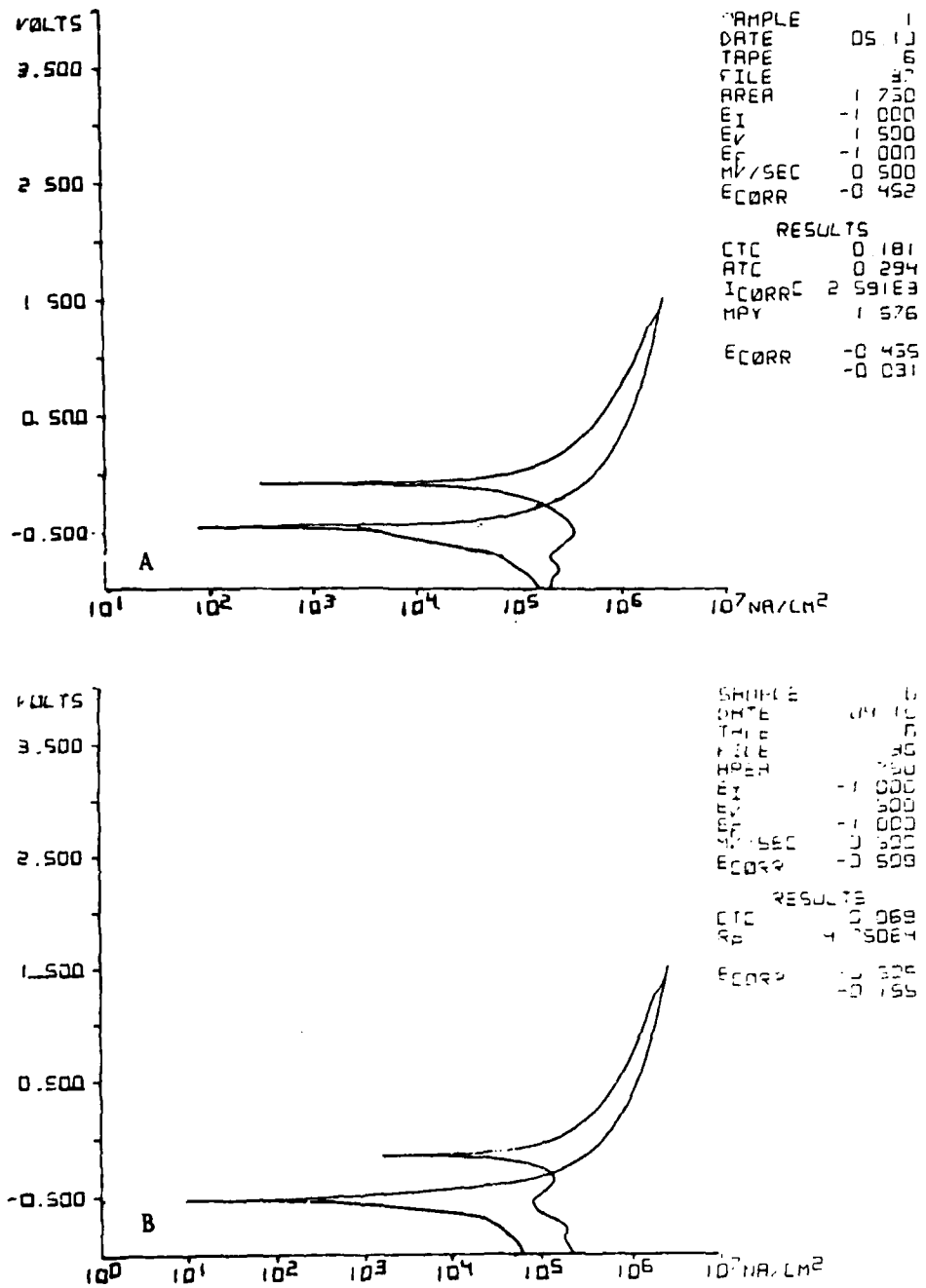

Fig. 3.3: Typical potentiodynamic polarization curves of commercial Pb-Sn coating 10^{-2}M NaCl. A. After laser treatment. B. As-deposited specimen.

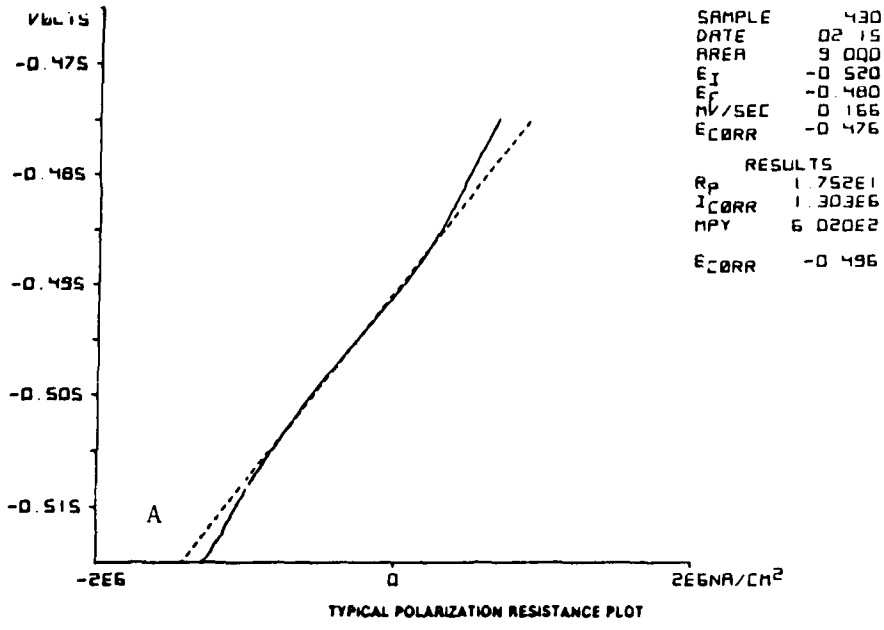

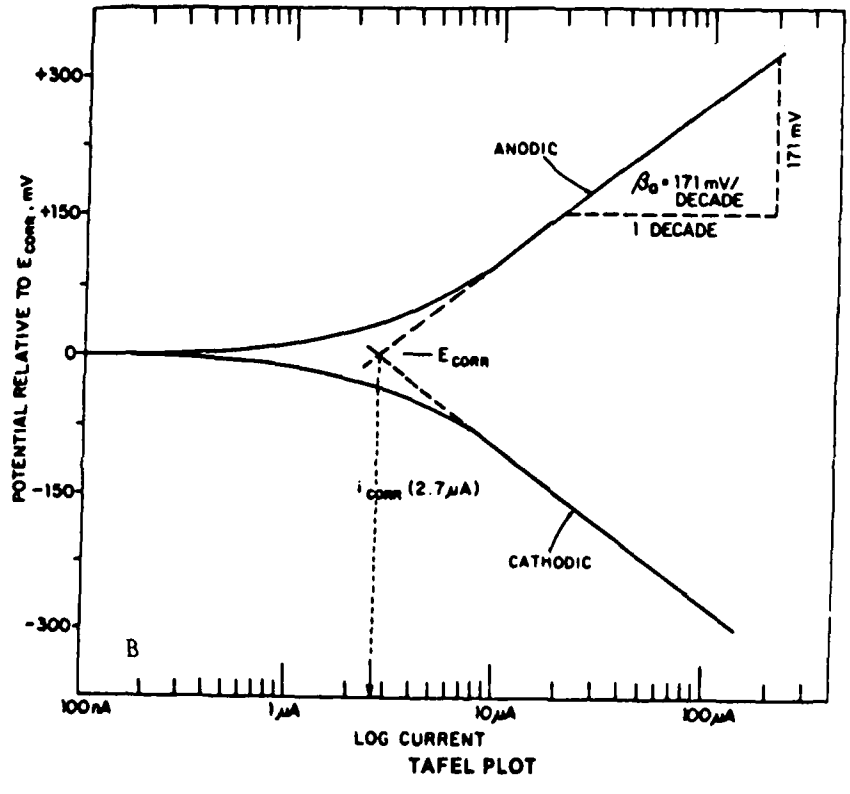

Fig. 3.4 : A. Typical linear polarization curve
B. Typical Tafel plot

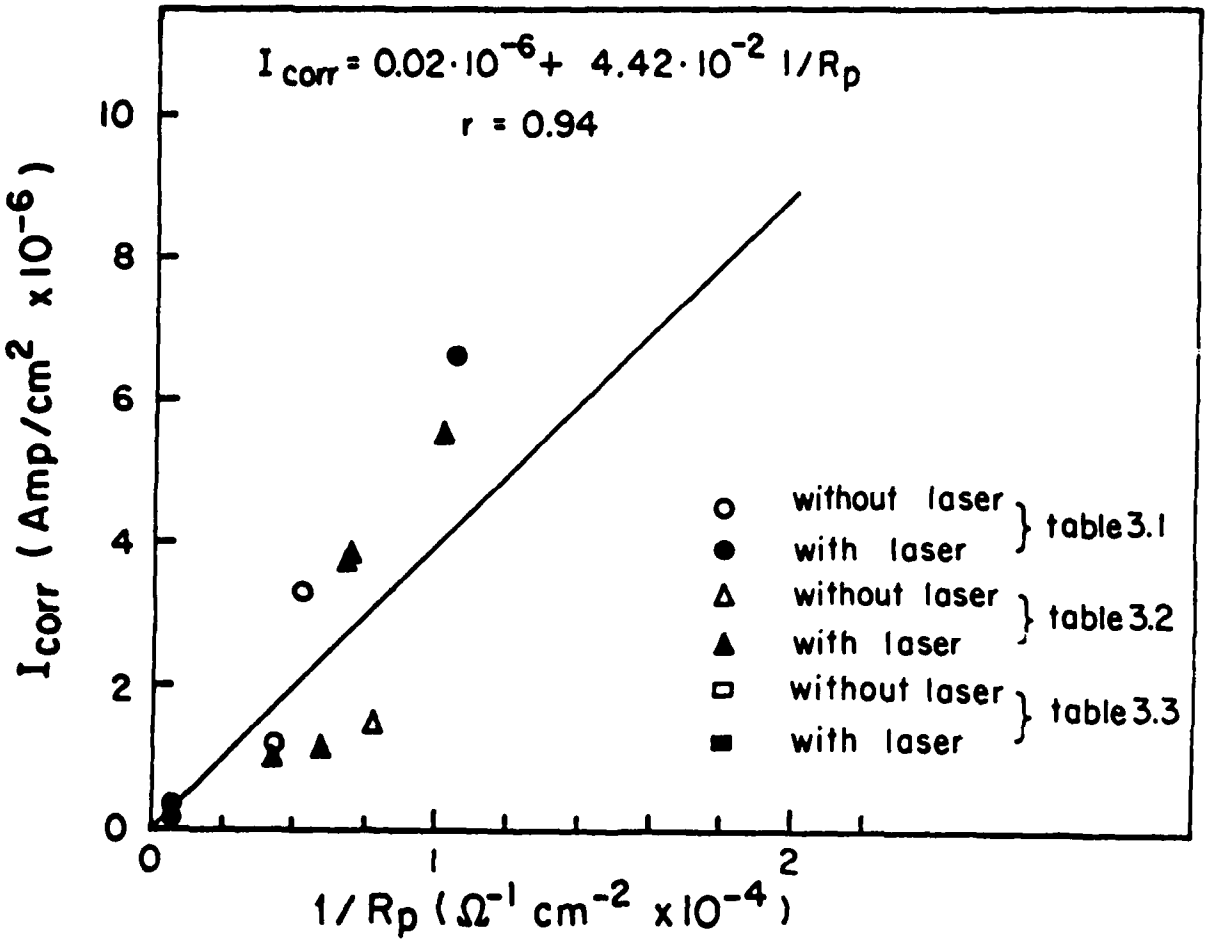

Fig. 3.5: Correlation obtained between I_{corr} and $1/R_p$ for polarization of Pb-Sn coating in 10^{-2}M NaCl

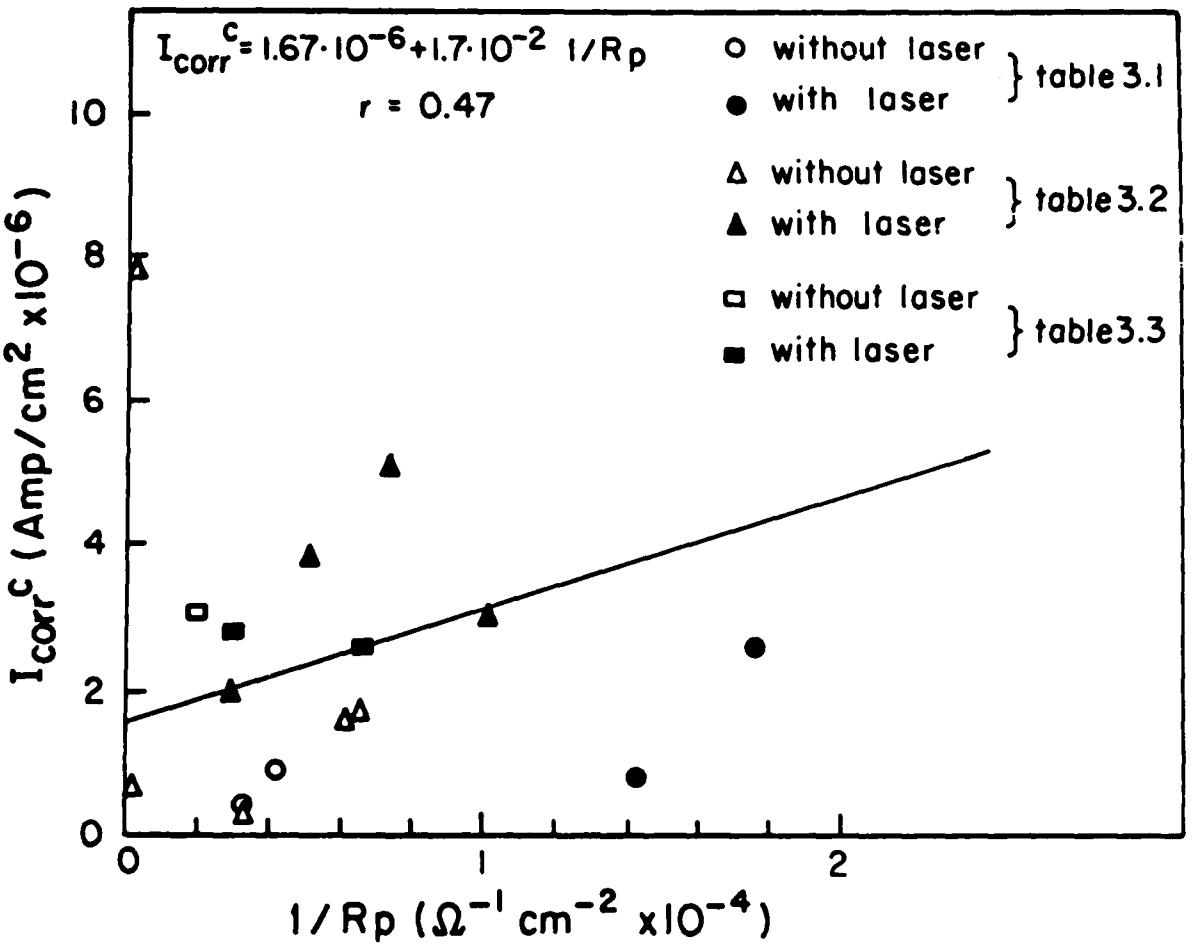

Fig. 3.6: Correlation obtained between I_{corr}^{c} and $1/R_p$ for polarization of Pb-Sn coating in 10^{-2}M NaCl

3.2 SEM Analysis

The micrographs are grouped according to the Tables: Figs. 3.7÷3.18 refer to Table 3.1, Figs. 3.19÷3.26 - to Table 3.2, Figs. 3.27÷3.29 - to Table 3.3, and Figs. 3.30÷3.35 to Table 3.4.

3.2.1 Laboratory Specimen

Fig. 3.7 shows the laser treated Pb-Sn coating with varying coating thickness, and Fig. 3.8 - the same specimens after polarization. EDS analyses of the various areas are given in Fig. 3.9.

The specimens without laser treatment before and after polarization are shown in Figs 3.10÷3.11, respectively. The EDS analyses of these specimens are shown in Fig. 3.12.

Comparison between the laser-treated and untreated specimens revealed that the laser treatment resulted in morphology changes. Separate brighter (Pb-rich) and darker (Sn-rich) zones were produced probably through a melting process.

The corroded areas of the laser treated and untreated specimens revealed similar phenomena of Pb-dissolution. While from the laser treated surfaces (Figs. 3.8, 3.9) Pb-rich zones were dissolved, Pb grains were dissolved from the as-deposited ones (Figs. 3.11, 3.12). The EDS analyses show the presence of Sn only at the corroded areas of both laser treated and untreated surfaces.

Figs. 3.13÷3.18 are cross-sections of the specimens shown in Figs. 3.57÷3.12. Figs. 3.13 and 3.14 revealed dissolution of Pb during polarization from untreated Pb-Sn coating. The elimination of the bright Pb-rich areas by the corrosion process was characterized by a pitting effect. (Figs. 3.14, 3.15).

The cross-sections of the laser-treated surfaces are shown in Figs. 3.16÷3.18. The development of different regions in

the coating is seen clearly. Fig. 3.16 shows a Sn-rich grey area and brighter areas with Pb and Sn content. Table 4.5 shows the concentration distribution over the depth of the brighter region. The Sn content of the grey region remained constant irrespective of depth.

Table 3.5: EDS analysis of the bright region shown in the laser treated Pb-Sn coating cross-section (see Fig. 3.16)

Element	Outer Side wt%	Center wt%	Near Cu basis wt%
Pb	45	78.4	39.9
Sn	49.6	11.8	21.7
Cu	5.4	9.8	38.4
Cl	0.0	0.0	0.0

Pb dissolution from the surface of the Pb-rich region was possibly responsible for the smaller amount of Pb on the outer side of the coating in compared with the center.

The phenomenon of Pb dissolution which resulted in exposed areas is seen in Fig. 3.17. The development of various regions is seen clearly also in the unpolarized specimen shown in Fig. 3.18.

Figs. 3.19÷3.24 bring out the intergranular mode of the corrosion process. Figs. 3.19 and 3.20 show the corroded area of Pb-Sn coating with 2.7μm thickness. Although the backgrounds of the corroded area differed, the mechanism seems to be similar dissolution of Pb from the grain boundaries spreading to the Pb-rich zone and further to the tin-rich area. Table 3.6 which shows the EDS analyses of the various areas support these observations.

Table 3.6: Comparison between EDS analyses of corroded Pb-Sn coating specimen (2.7μm in thickness) with and without laser treatment

	Uncorroded Specimens						Corroded Specimens			
	All Area wt%		Bright Region wt%		Dark region wt%		Edge Corr. Area wt%		Center Corr. Area wt%	
	*	**	*	**	*	**	*	**	*	**
Pb	52.0	50.5	91.1	***	9.7	***	3.8	14.7	3.6	8.4
Sn	43.3	46.8	5.8	***	87.5	***	74.3	77.2	36.7	38.9
Cu	2.5	2.5	0.1	***	0	***	21.8	8.0	59.5	52.6
Cl	0.2	0.2	3.0	***	2.8	***	0.1	0.1	0.2	0.1

* Laser treated specimen

** Untreated laser specimen

*** Not obvserved in as-deposited laser specimen

Figs. 3.21 and 3.22 and Table 3.7 show a similar pattern for the Pb-Sn coating with 8.4μm thickness.

Table 3.7: Comparison between the EDS analyses of the corroded Pb-Sn coating specimen (8.4μm) with and without laser treatment

	Uncorroded Area wt%		Corroded Area wt%	
	*	**	*	**
Pb	53.6	51.1	7.4	4.2
Sn	46.1	48.6	49.6	44.2
Cu	0.0	0.1	42.8	51.5
Cl	0.3	0.2	0.2	0.1

* Laser treated specimen

** As-deposited specimen.

The same corrosion mode was observed also for the coating thickness of 12.7μm (Figs. 3.23, 3.24). The "B" micrographs show distinctly the boundary of the corroded area as only Sn crystals remain on the copper base.

All experiments discussed above were conducted by irradiation by unfocused laser. In order to achieve higher laser energis, the beam was cofused and $6 \cdot 10^7 watt/cm^2$ was applied per pulse. Figs. 3.25, 3.26 are SEM micrographs of these specimens. A very bright surface was achieved with distinct separation between the bright Pb-rich and grey Sn-rich areas, (Figs. 3.25, 3.26). The surface obtained was smoother than its as-deposited counterpart as can be seen by comparing Figs. 3.25B and 3.25D against 3.25E. Experiments will be conducted to study the effect of high laser energy on the corrosion resistance of Pb-Sn coatings.

3.2.2 Commercial Specimens

Figs. 3.27A through D are micrographs of the commercial specimens treated at different laser energy, and Fig. 3.27E the untreated specimen. Fig. 3.28 shows the same micrographs at higher magnification. It is seem that a melting process occurred, but there is only partial separation between the bright and grey areas. The best smoothing of the surface was achieved with higher laser energy per pulse. Table 3.8 reveals this separation for specimens (1) and (3) (Figs. 3.28A and 3.28C). The composition of the as-deposited specimen is also included in Table 3.8 (specimen O for which no separation was observed, Fig. 3.8E).

Table 3.8: Comparison of different areas in Pb-Sn commercial specimen after laser treatment

	(1)			(2)		(0)
	Total	Bright Area Grain Center wt%	Grain Edge wt%	Bright Area wt%	Grey Area wt%	Total wt%
Pb	50.9	76.9	25.6	78.7	22.1	48.6
Sn	47.3	21.9	72.5	20.6	76.9	49.6
Cu	1.8	1.2	1.9	0.7	1.0	1.8

Figs. 3.29 are the micrographs of the corroded commercial specimen; Figs. 3.29A and 3.29B show the laser treated area, and Fig. 3.29C the as-deposited area after polarization. Table 3.9 summarizes the EDS analyses of the specimen after polarization.

Table 3.9: EDS analysis results of Pb-Sn coating after polarization

	Without laser treatment (0)			Laser treated (1)	
	Small wt%	Larger Crystal wt%	Whole Area wt%	Whole Area wt%	Between Crystals wt%
Pb	0.6	1.5	5.0	2.9	7.3
Sn	21.4	88.8	47.2	71.0	57.3
Cu	73.9	7.16	46.0	24.1	1.2
Cl	4.1	2.1	1.8	2.0	34.1

These results and SEM observations show that the corrosion process begins initially with Pb dissolution followed by partial Sn dissolution. It was observed that the amount of Sn remaining on the base was higher for the laser treated surface compared with the as-deposited surface, 71% against 47.2%, respectively (Table 3.9).

This phenomenon can possibly be attributed to the laser treatment.

3.2.3 Tin Coated Specimens

Figs. 3.30÷3.35 are micrographs of the as-deposited tin coating after laser treatment and after polarization. Figs. 3.30 show the coating (thickness-6.7μm) before and after laser treatment. The melting phenomenon is demonstrated clearly by the transition from Fig. 3.30A to 3.38B. Higher magnification of the laser treated area (Fig. 3.30B) revealed the effect of cooling on the melted surface (C,D).

Figs 3.31-3.32 and 3.34-3.35 compare the corroded as-deposited and laser treated surfaces for coating thicknesses of 1μm and 3.6μm respectives. It is seen that the corrosion morphology of both surfaces has a circular symmetry. Initially, the circular boundaries separated from the background and afterwards tin dissolution occurred. The corroded area composition shows a of small amount of Cl, and larger amounts of Cu and Sn (Figs. 3.32A,C).

4. CONCLUSION

Laser induced melting of the Pb-Sn coating resulted in bright area at energy levels of 10^6watt/cm^2 - 10^7watt/cm^2 per pulse. The laser treated area produced a lead-rich zone believed to be α solid grain as discussed in the previous report. Formation of these zones possibly prevents improvement in corrosion resistance and affects the corrosion mode by producing larger anodic sites. Perferential dissolution of lead was observed for both the as-deposited and laser treated specimens, resulting in a non-general corrosion mode closer to the intergranular type.

Calculations showed the laser-treated specimen had higher corrosion rates than their as-deposited counterparts. Analysis of the results revealed inconsistencies discrepancies, possibly due to deviation of the corrosion mode from the general type.

The commercial Pb-Sn coated specimens revealed the same corrosion behavior as the laboratory-plated ones. The corrosion resistance of the as-deposit of tin coated specimen was found also to be higher than for the laser-treated specimen.

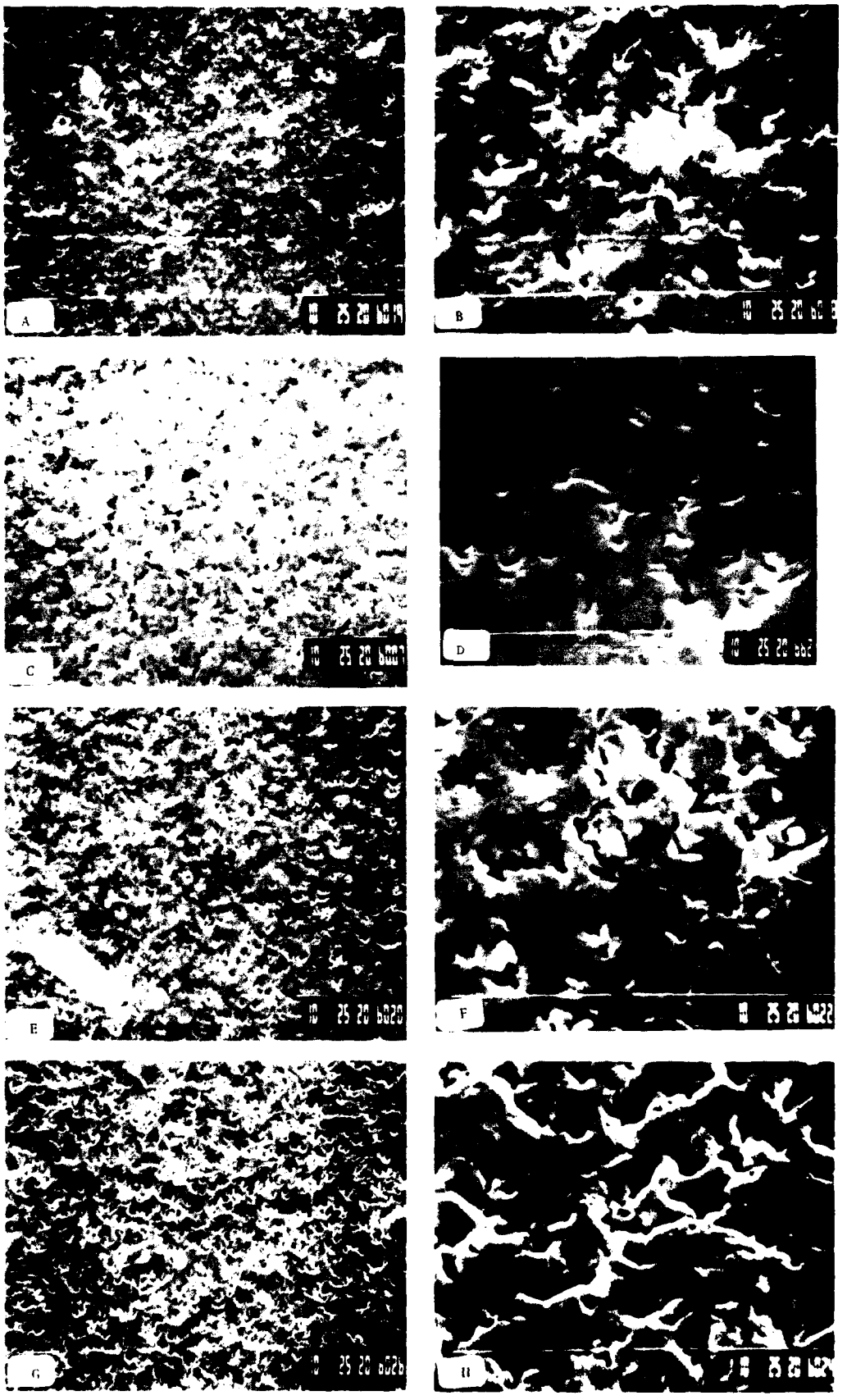

Fig. 3.7 SEM observations of Pb-Sn coating after laser treatment.

A,B 1.89µm x 1000, x 5000.
C,D 2.1 µm x 1000, x 5000
E,F 4.3 µm x 1000, x 5000
G,H 12.7 µm x 1000, x 5000

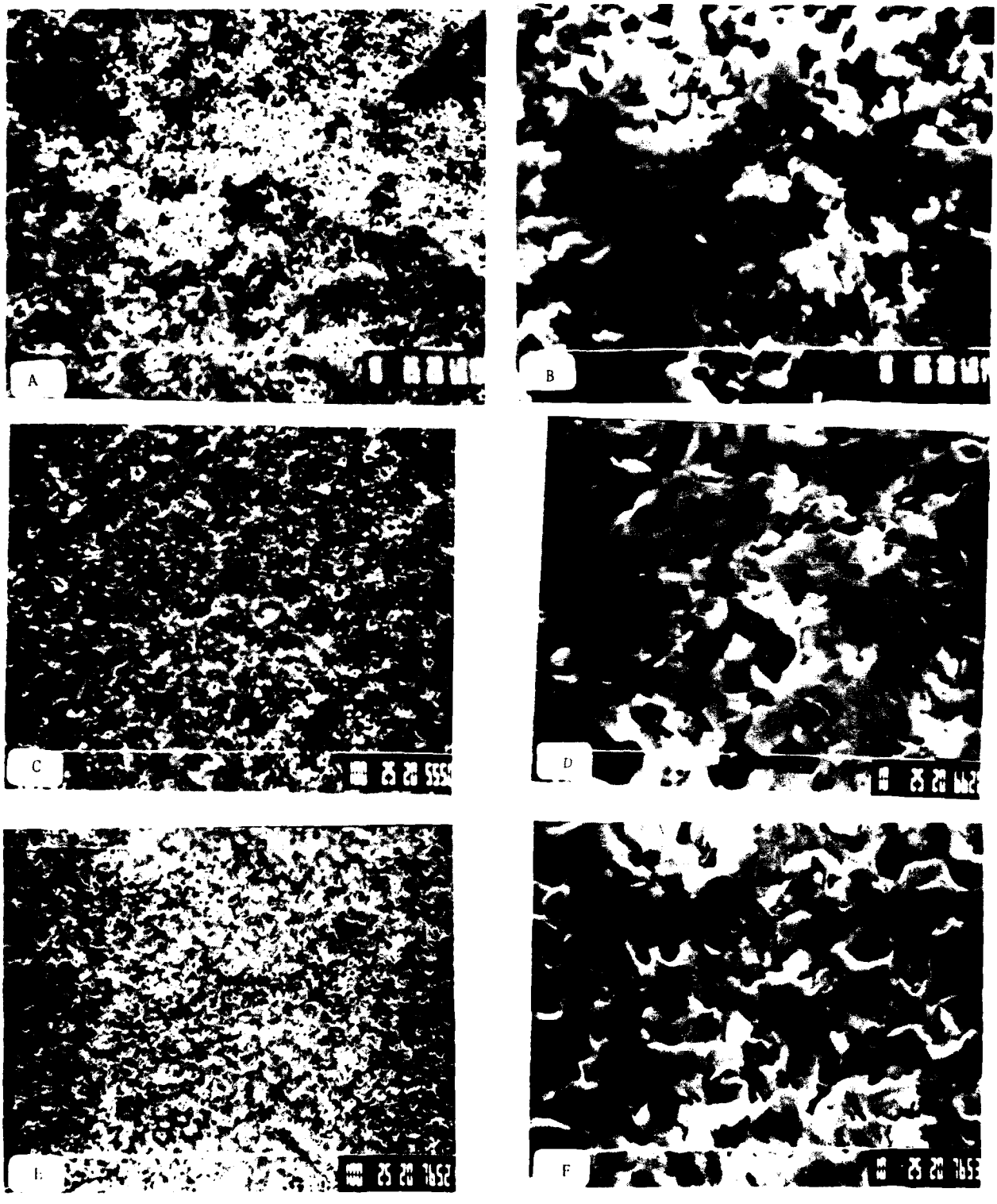

Fig. 3.8 SEM observations of laser treatment Pb-Sn surfaces after potentiodynamic polarization in 10^{-2}M NaCl

A,B 1.89μm x 1000, x 5000
C,D 2.1 μm x 750, x 5000
E,F 8.1 μm x 750, x 5000

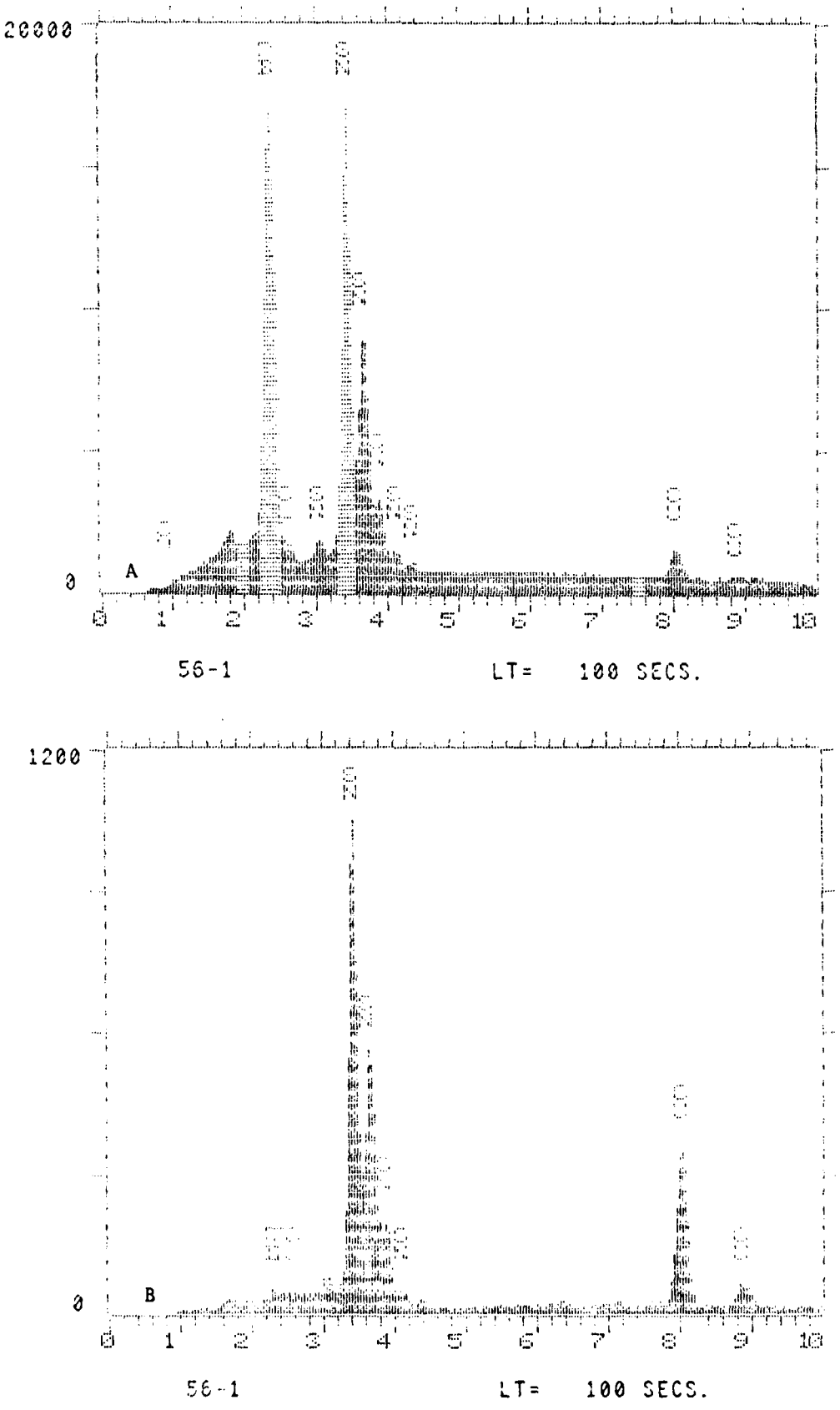

Fig. 3.9 EDS analysis of laser treated surface 2.1μm before and after polarization in 10^{-2}M NaCl.
A. Before corrosion (Fig 3.7C)
B. After corrosion (Fig 3.8)

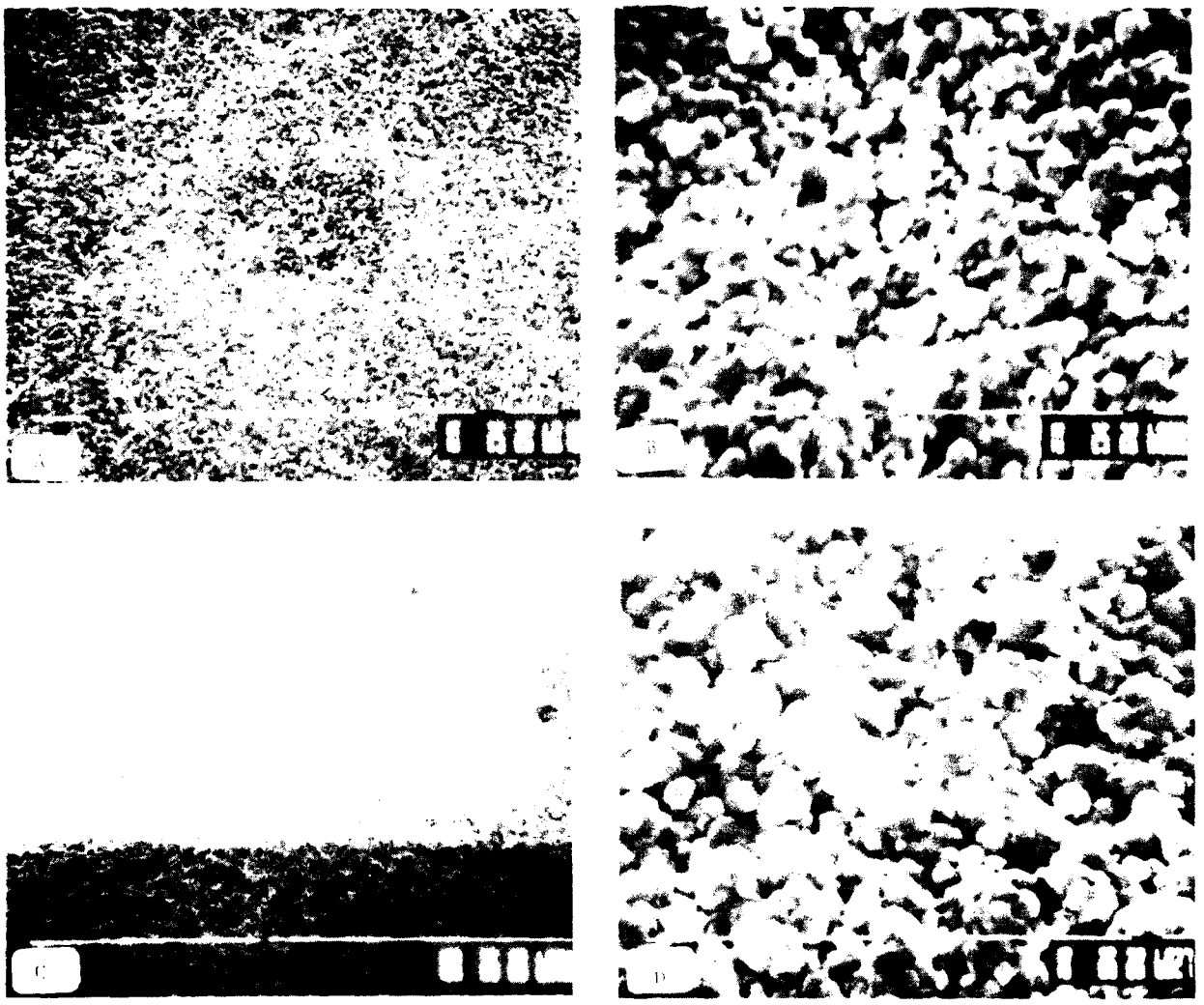

Fig. 3.10 SEM observasions of as-deposited coatings
A,B. 2.1 µm x 1000, x 5000
C,D. 12.7µm x 1000, x 5000

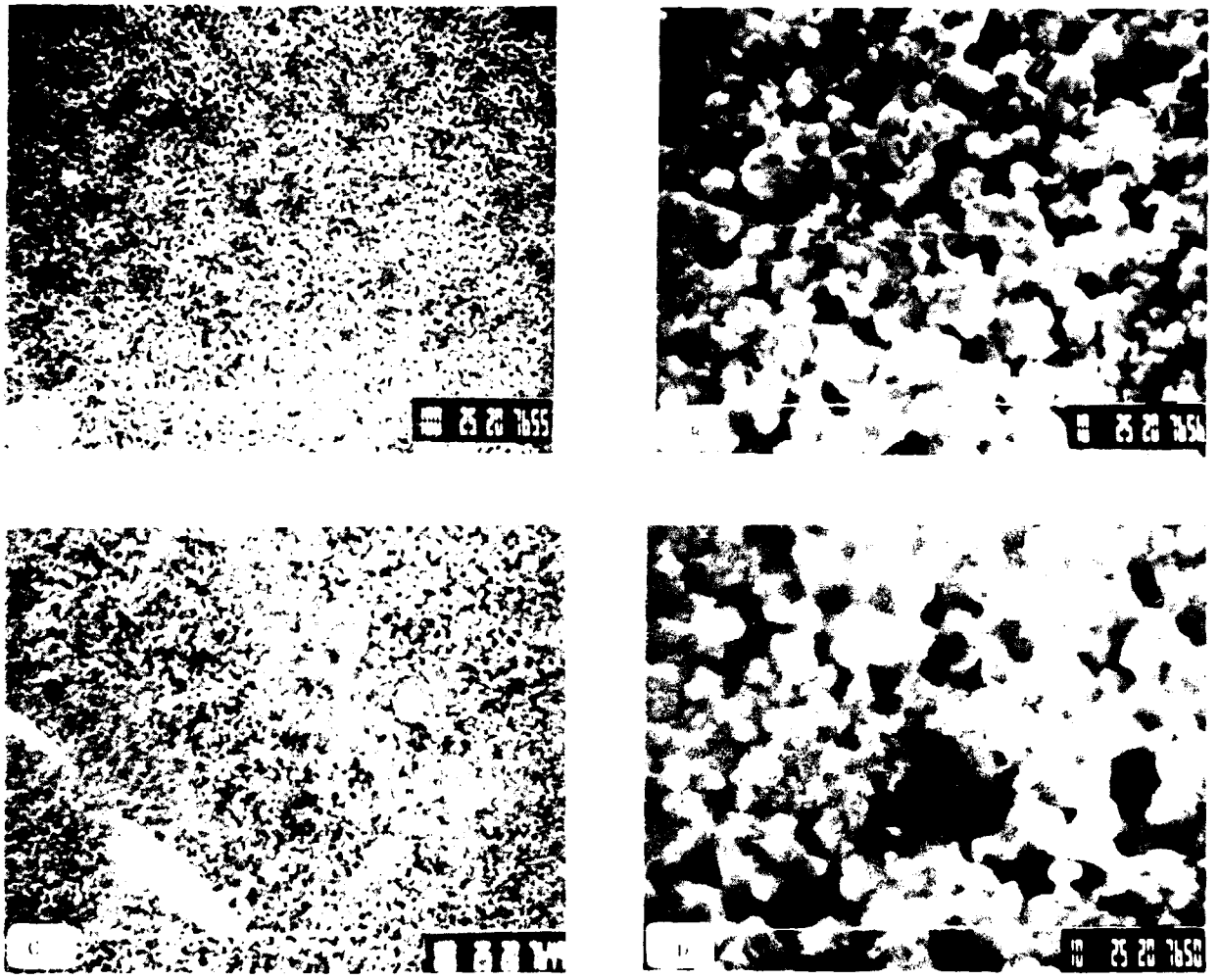

Fig. 3.11 SEM observations of corroded area of as-deposited Pb-Sn coatings with various after thickness polarization in 10^{-2}M NaCl.

A,B. 1.96 µm Pb-Sn coating thickness specimen.
x 750, x 5000respectively
C,D. 4.3 µm -Sn coating thickness specimen
x 750, x 5000 respectively

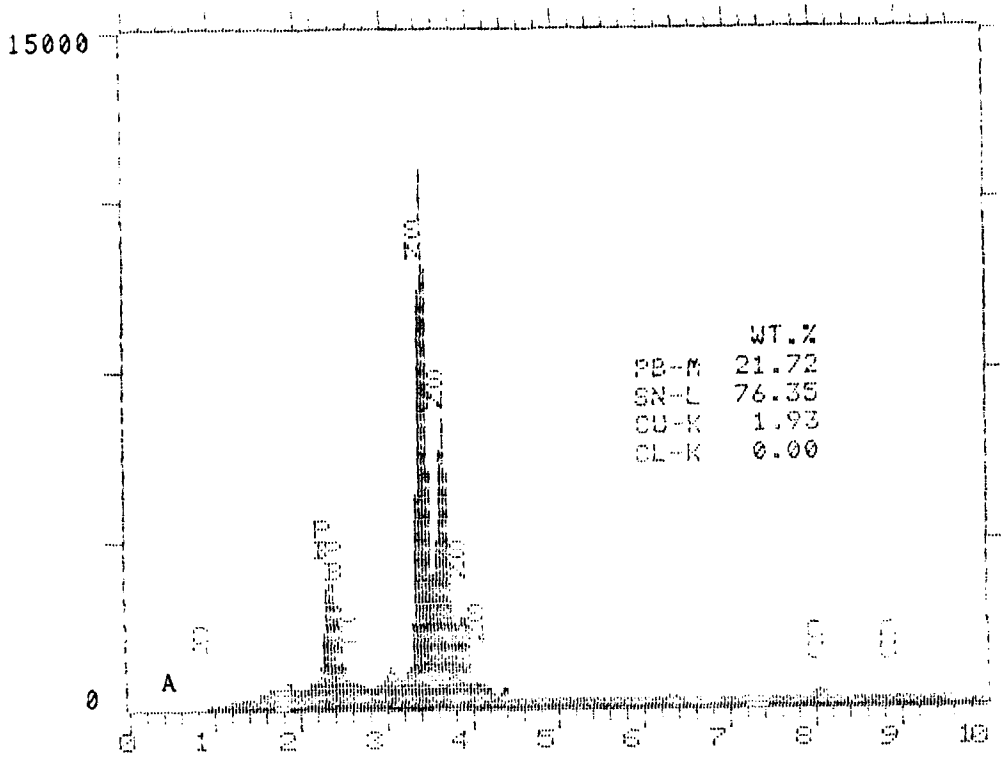

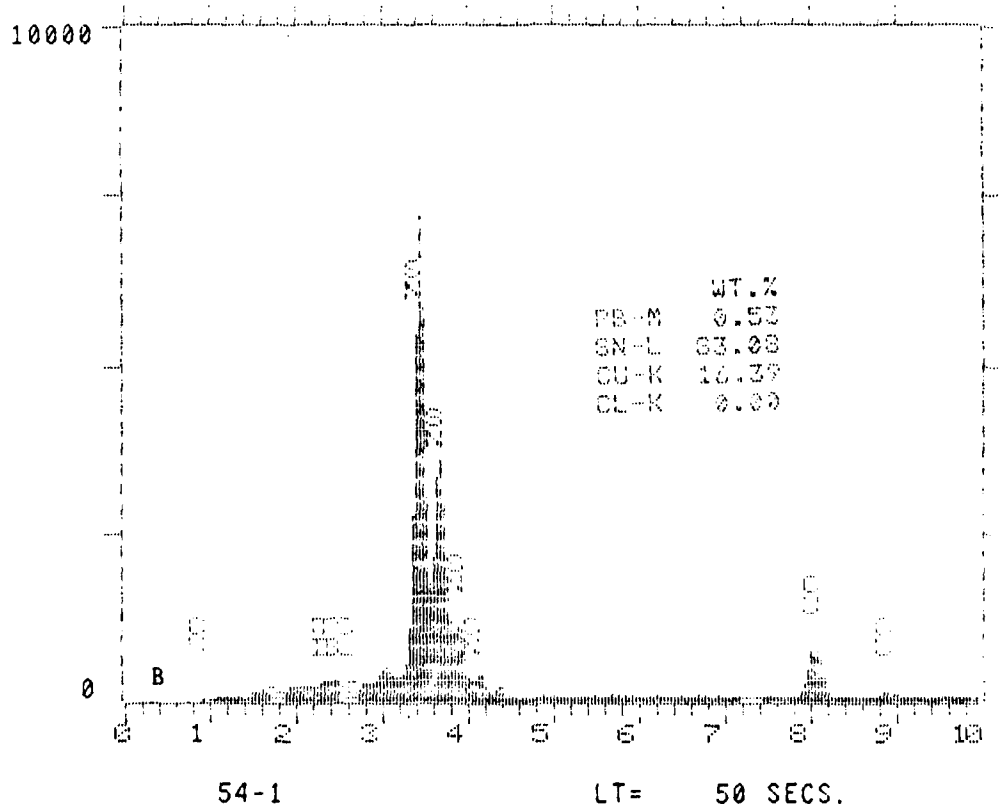

Fig. 3.12 EDS analysis of as-deposited Pb-Sn coating after polarization in 10^{-2}M (see Fig 4.11)

A. Coating thickness 1.96μm (Fig 4.1B).
B. Coating thickness4.3μm (Fig 4.11D)

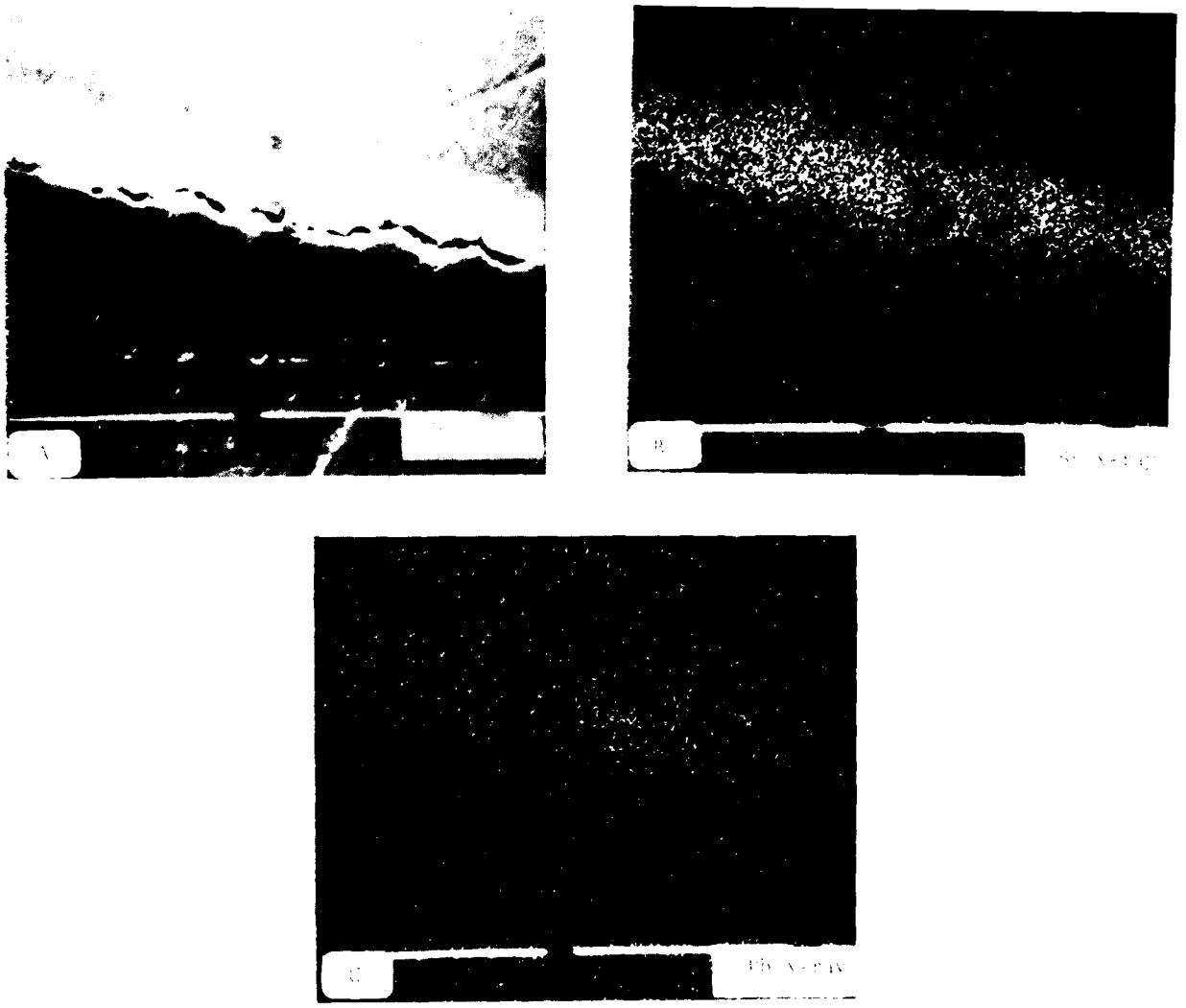

Fig. 3.13 SEM observations of cross-section of as-deposited Pb-Sn coating after polarization in 10^{-2}M NaCl (1.96µm thickness).

A. Corroded area x 5000.
B. Sn X-ray mapping of A.
C. Pb X-ray mapping of A.

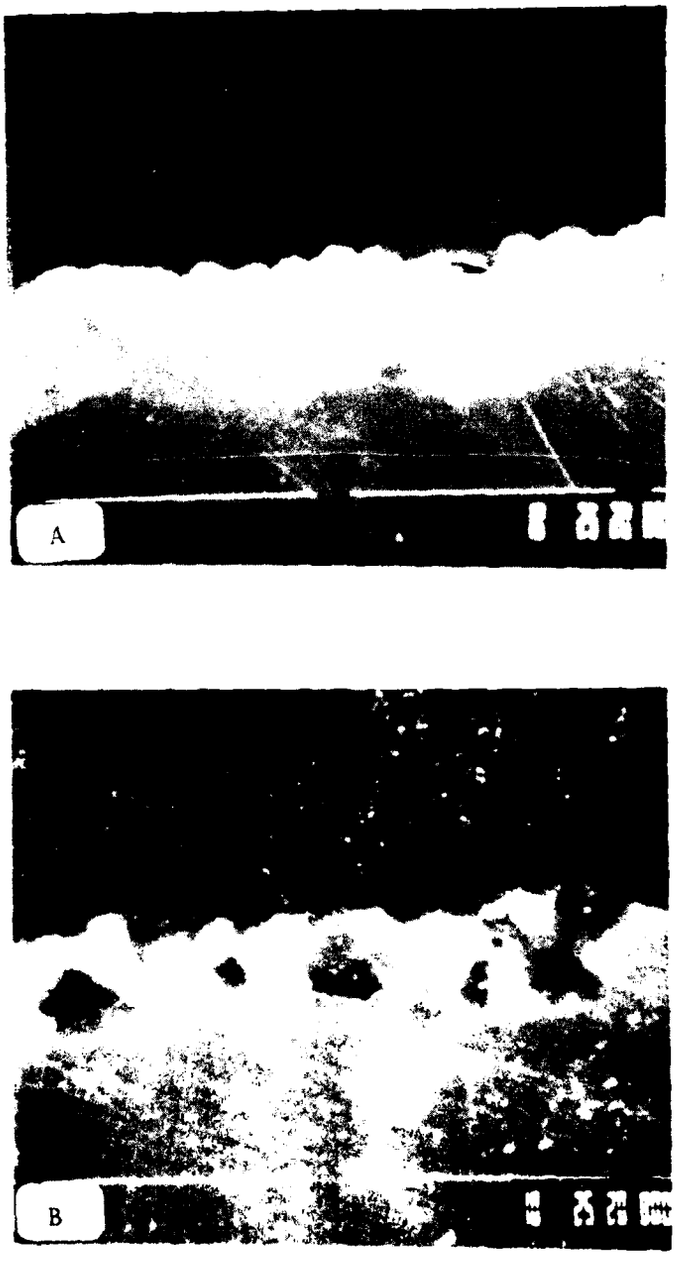

Fig. 3.14 SEM observations of cross-section of as deposited Pb-Sn coating after polarization in 10^{-2}M NaCl.
A. Uncorroded area. x 5000
B. Corroded area . x 5000

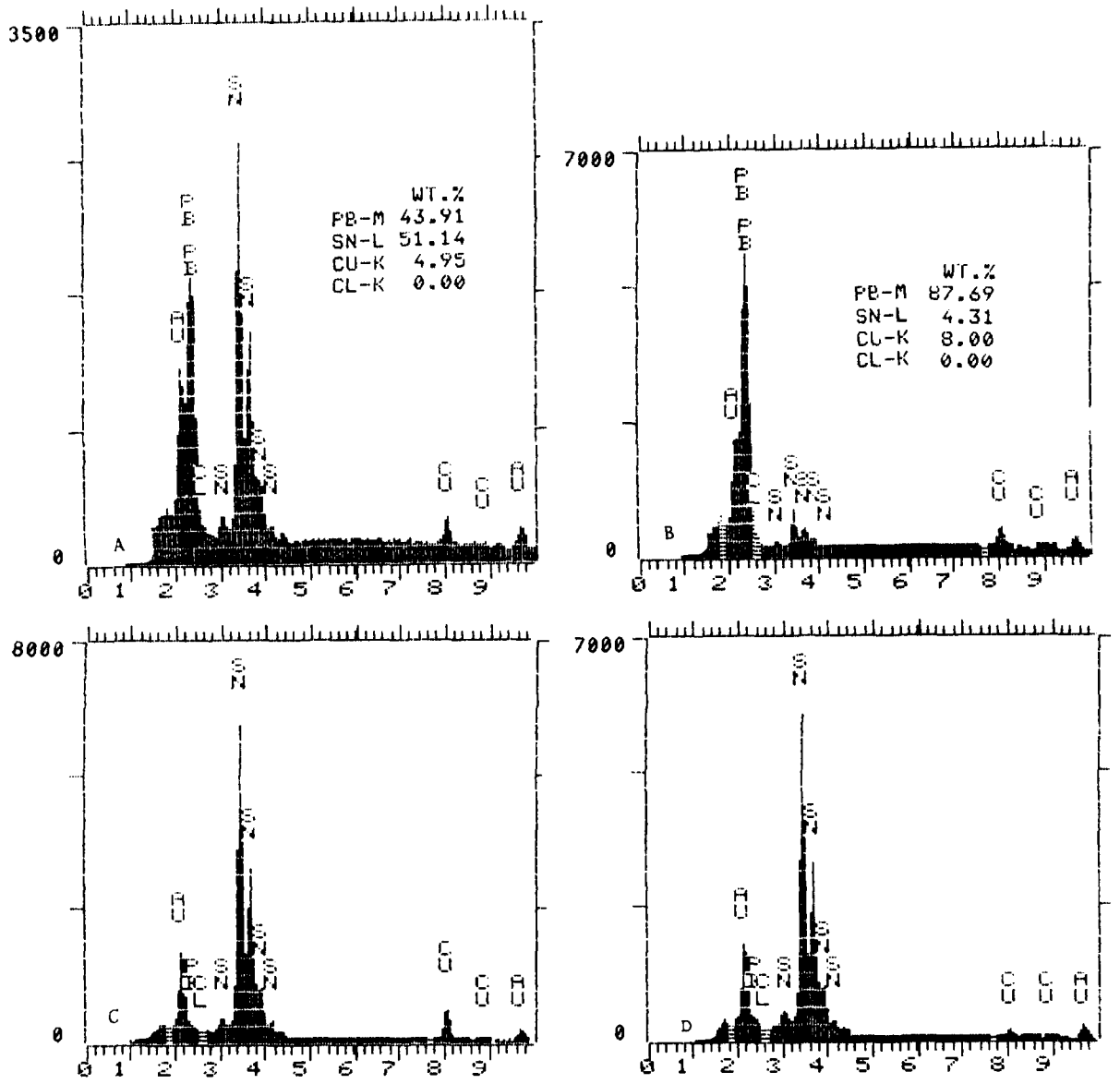

Fig. 3.15 EDS analysis of the area shown in Fig 4,14.

A. Uncorroded area(Fig 4.14A)
B. Uncorroded area bright region (Fig. 4.14A)
C. Uncorroded area grey region (Fig. 4.14A)
D. Corroded area (Fig. 4.14B).

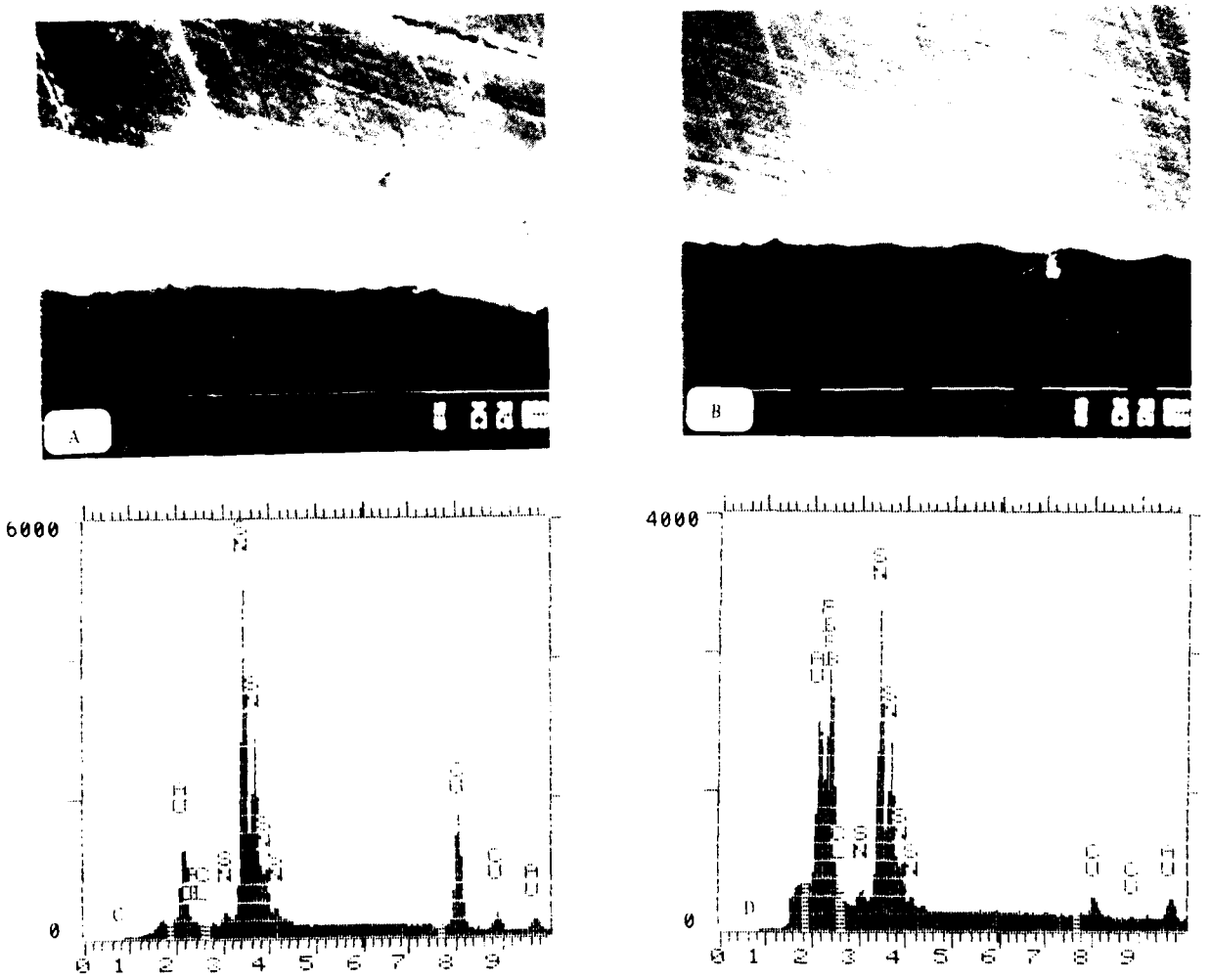

Fig. 3.16 SEM observations of Pb-Sn cross-section of laser treated specimen after polarization in 10^{-2}M NaCl (coating thickness 4.3µm)
A. Crossection observation x 5000
B. Crossection observation. x 2000
C. E.D.S analysis of the grey area.
D. E.D.S analysis of the bright area.

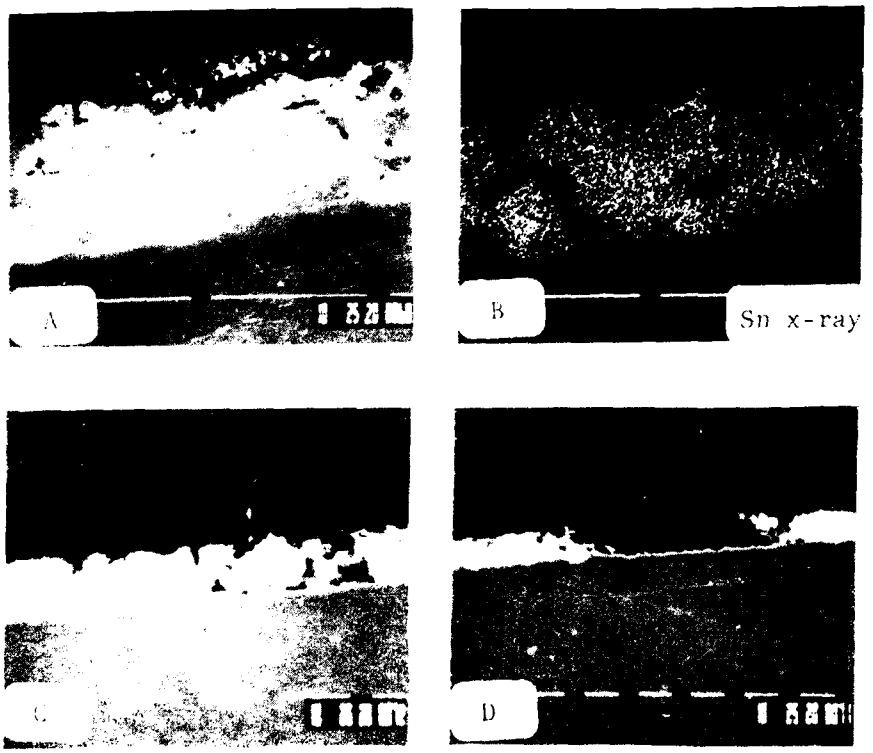

Fig. 17 SEM observations of cross-section of laser treated Pb-Sn specimen, after polarization in 10^{-2}M NaCl (Coating thickness 8.1μm).

A. Corroded area x 5000
B. Sn X-ray of A.
C. Corroded area x 2000
D) Corroded area x 1000.

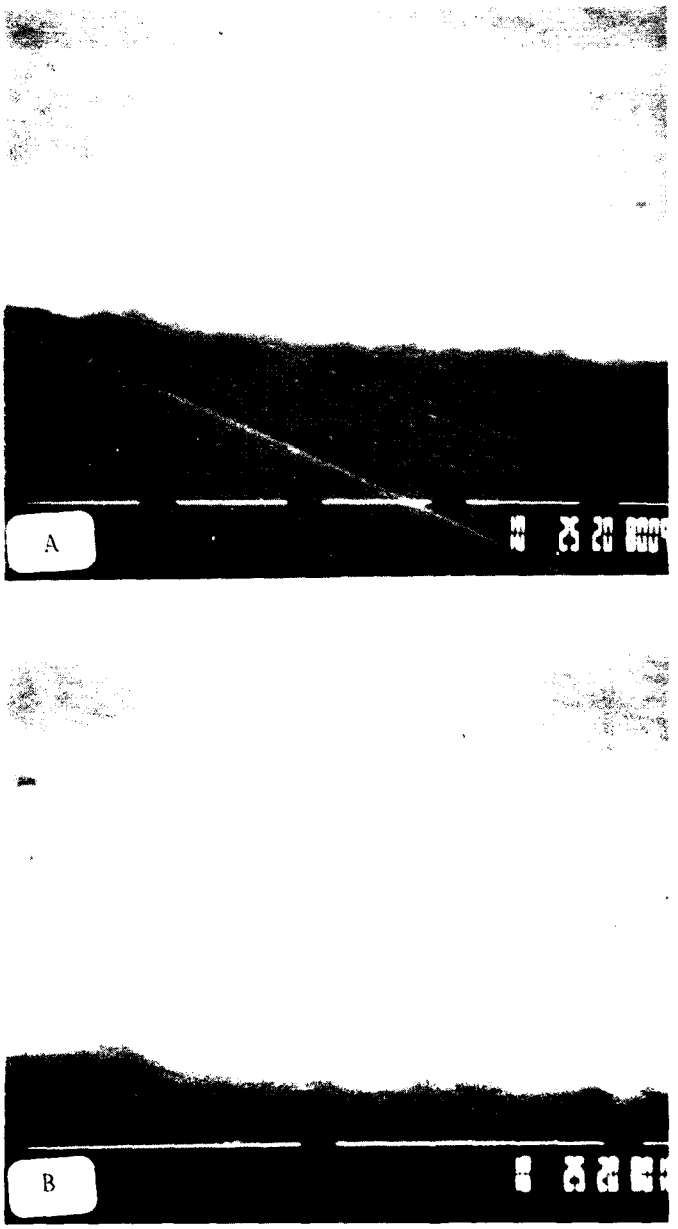

Fig. 3.18 SEM observations of cross-section of Pb-Sn laser treated specimen without polarization. (Coating thickness 12,7µm)

A. x 2000
B. x 5000

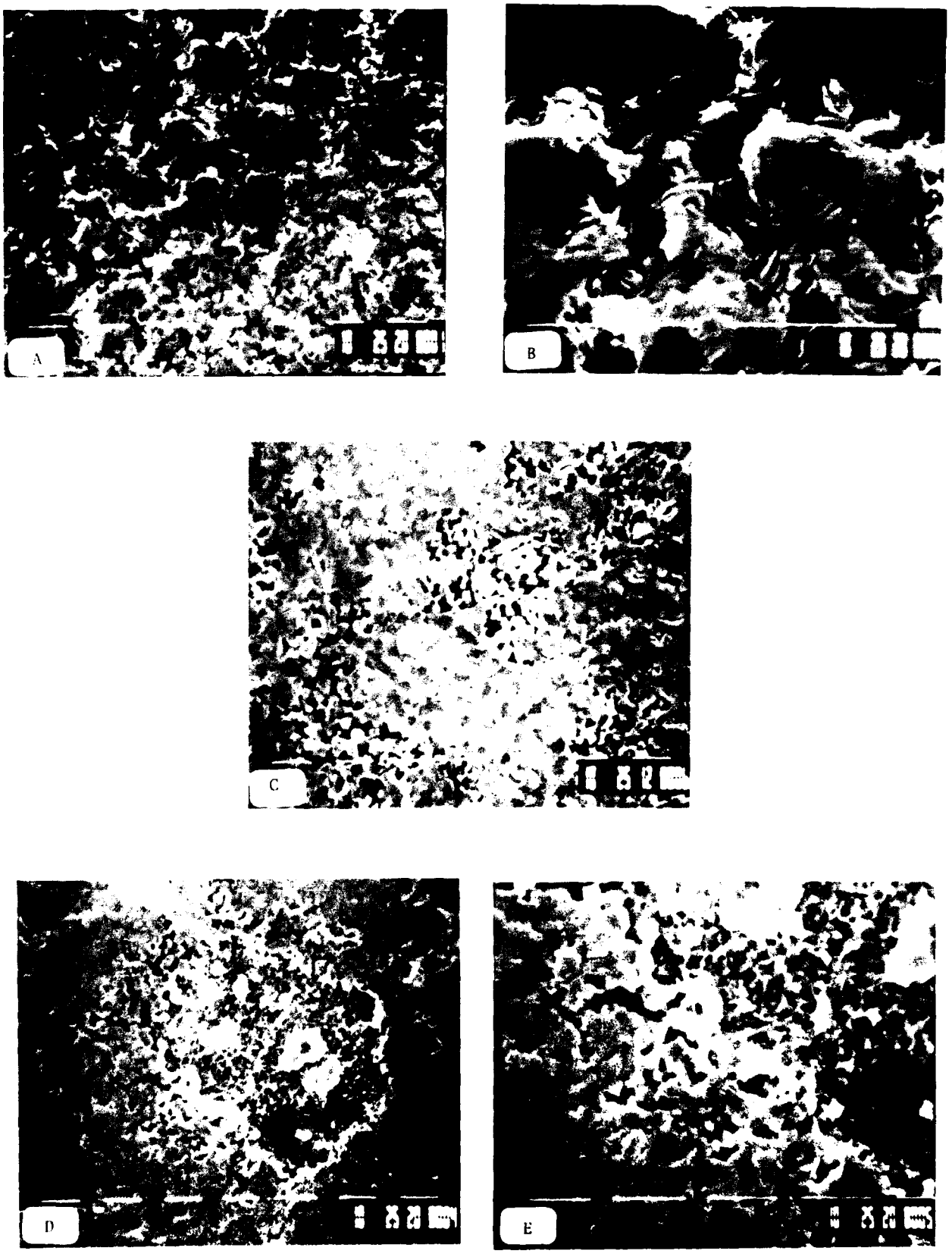

Fig. 3.19 SEM observations of Pb-Sn laser treated specimen after polarization in 10^{-2}M NaCl(coating thickness 2.7μm).

A. Corroded area x 1000
B. Corroded area x 5000
C. Corroded area x 1000
D. Corroded area x 1000
E. Corroded area x 2000

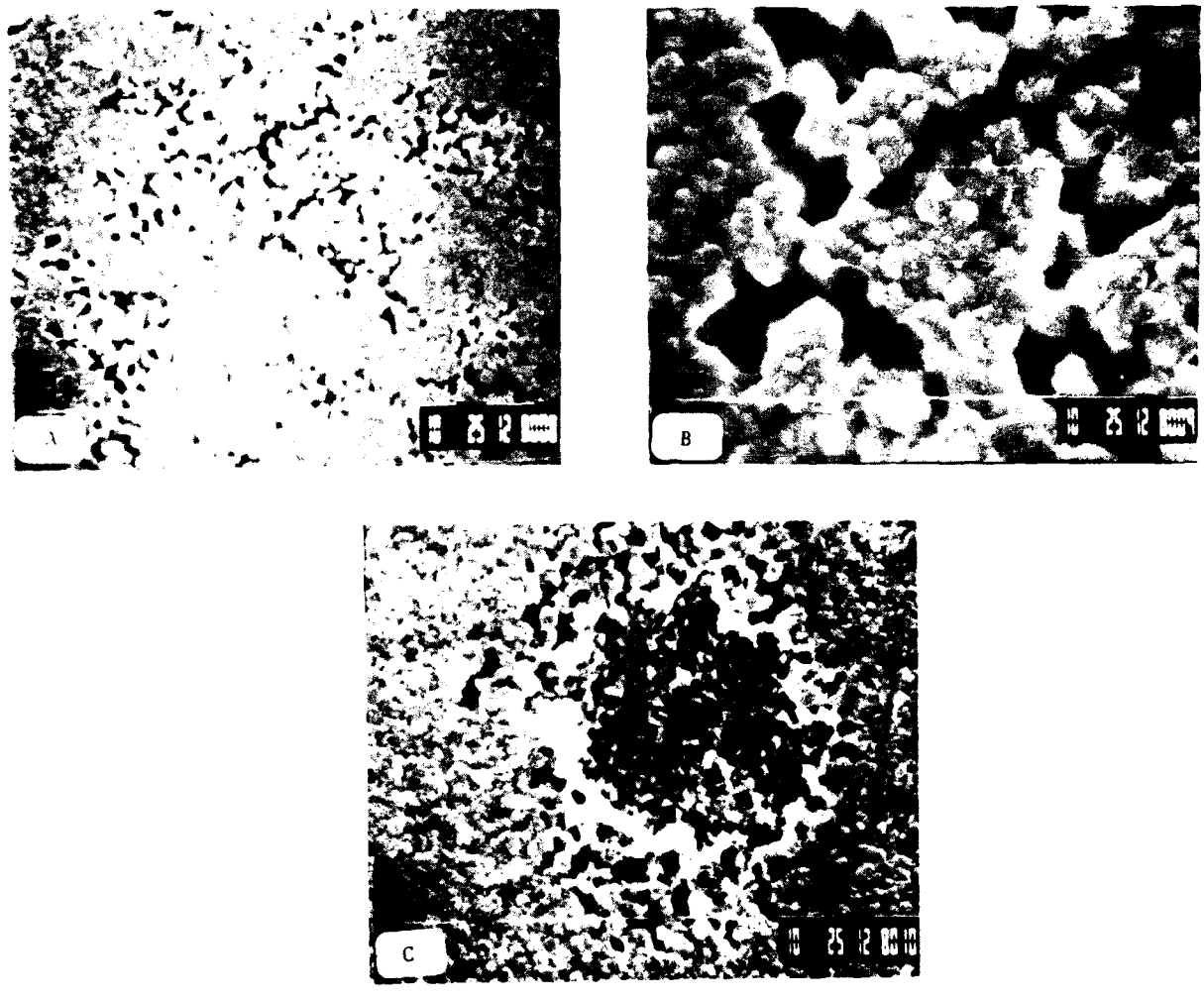

Fig. 3.20 SEM observations of corroded area of as deposited Pb-Sn coating after polarization in 10^{-2}M NaCl. (Coating thickness 2,9µm.

A. Corroded area x 1000.
B. Corroded area x 5000
C. Corroded area x 2000

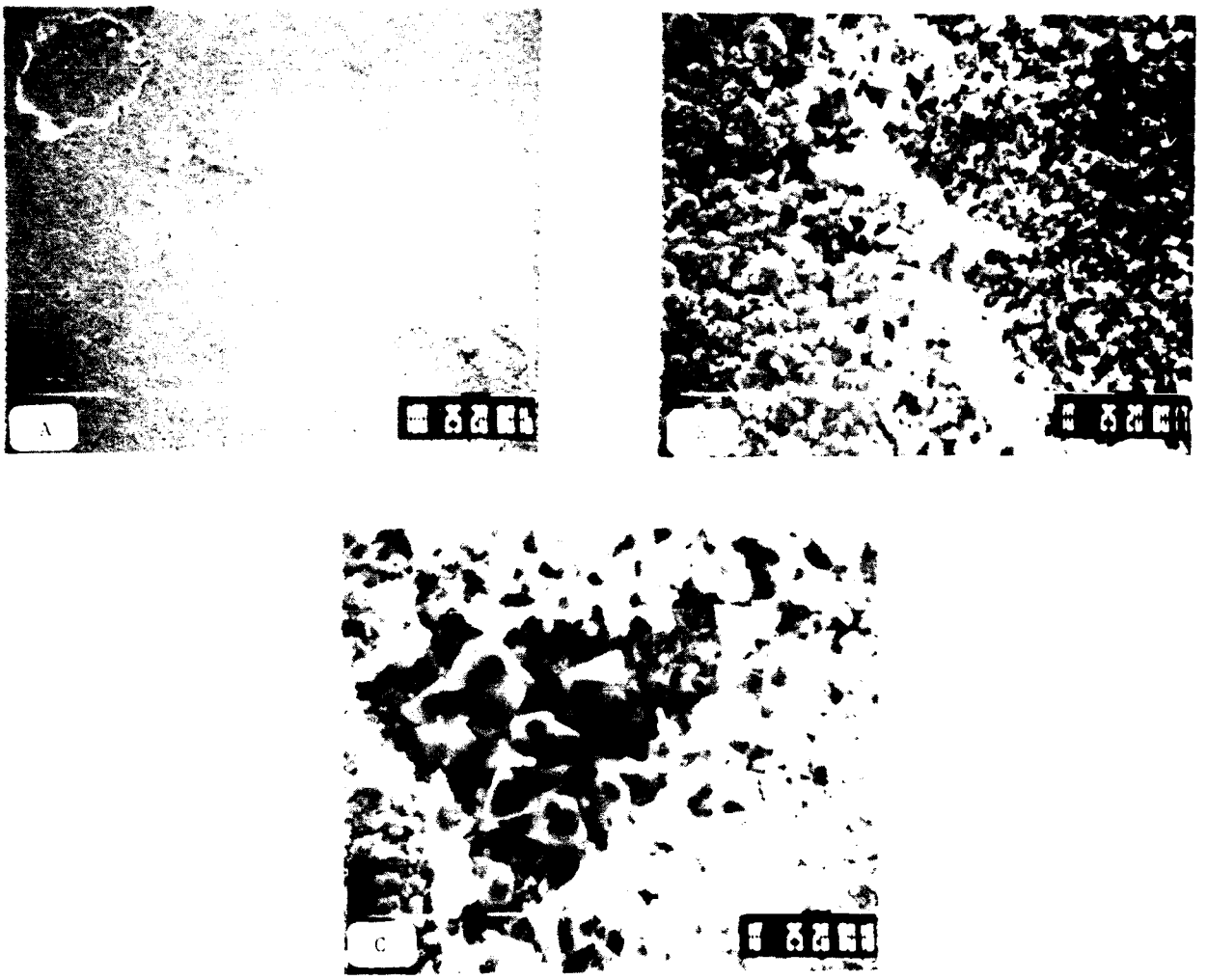

Fig. 3.21 SEM observations of corroded area of as deposited Pb-Sn coating after polarization in 10^{-2}M NaCl. (Coating thickness 8.4μm)

A. Corroded area x 200.
B. Enlargment of corroded area x 2000.
C. Beginning of corroded area x 2000.

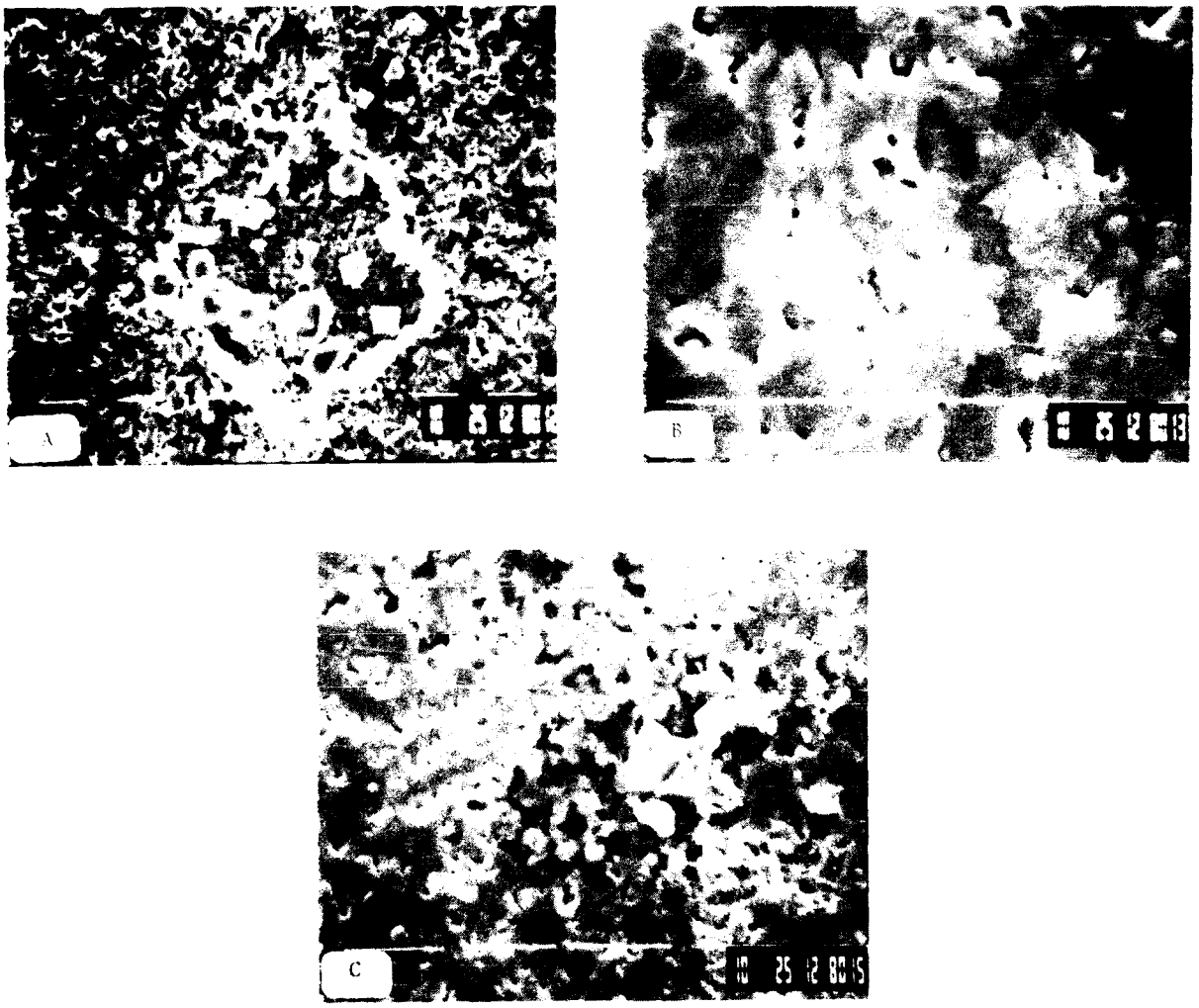

Fig. 3.22 SEM observations of Pb-Sn corroded area of laser treated specimen after polarization in 10^{-2}M NaCl.(Coating thickness 8.4µm).

A. Corroded area x 1000
B. Corroded area x 5000
C. Beginning of corrosion, Sn crystal x 2000.

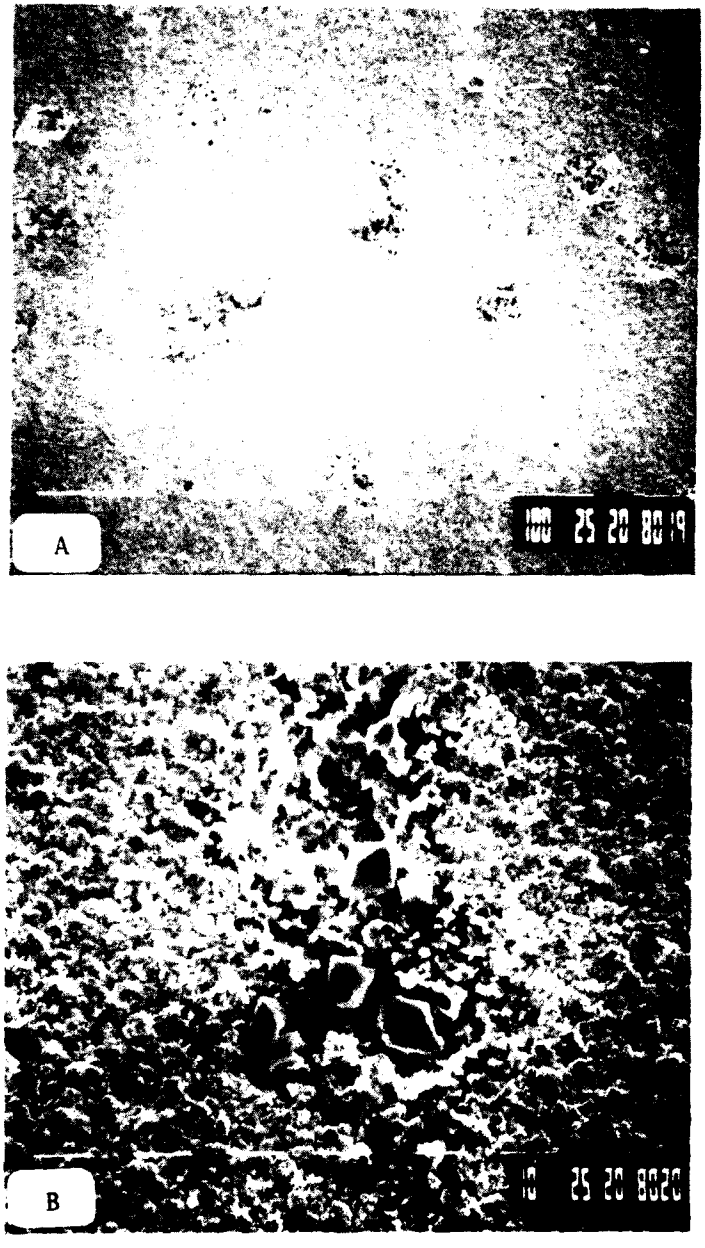

Fig. 3.23 SEM observations of corroded area of as deposited Pb-Sn specimen after polarization in 10^{-2}M NaCl.(Coating thickness 12.7μm).

A. Corroded area x 200.
B. Beginning of corroded area x 1000.

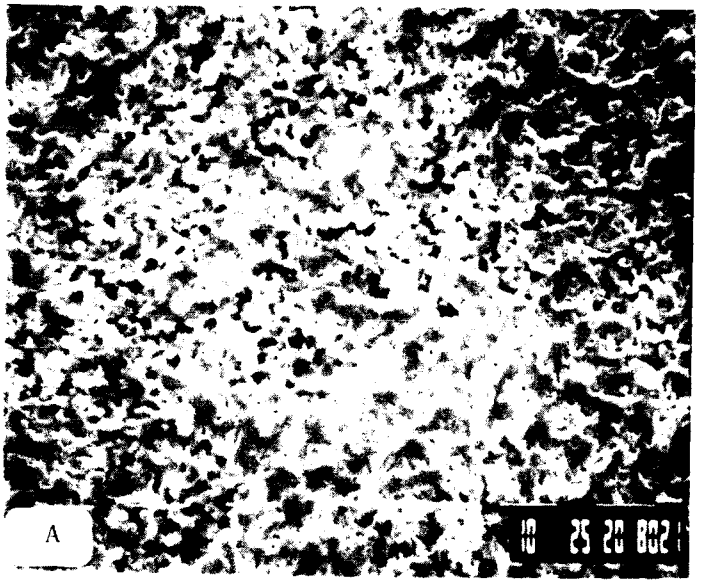

Fig. 3.24 SEM observation of corroded Pb-Sn laser treated specimen after polarization in 10^{-2}M NaCl.

A. Corroded area x 100.
B. Corroded area x 7500.

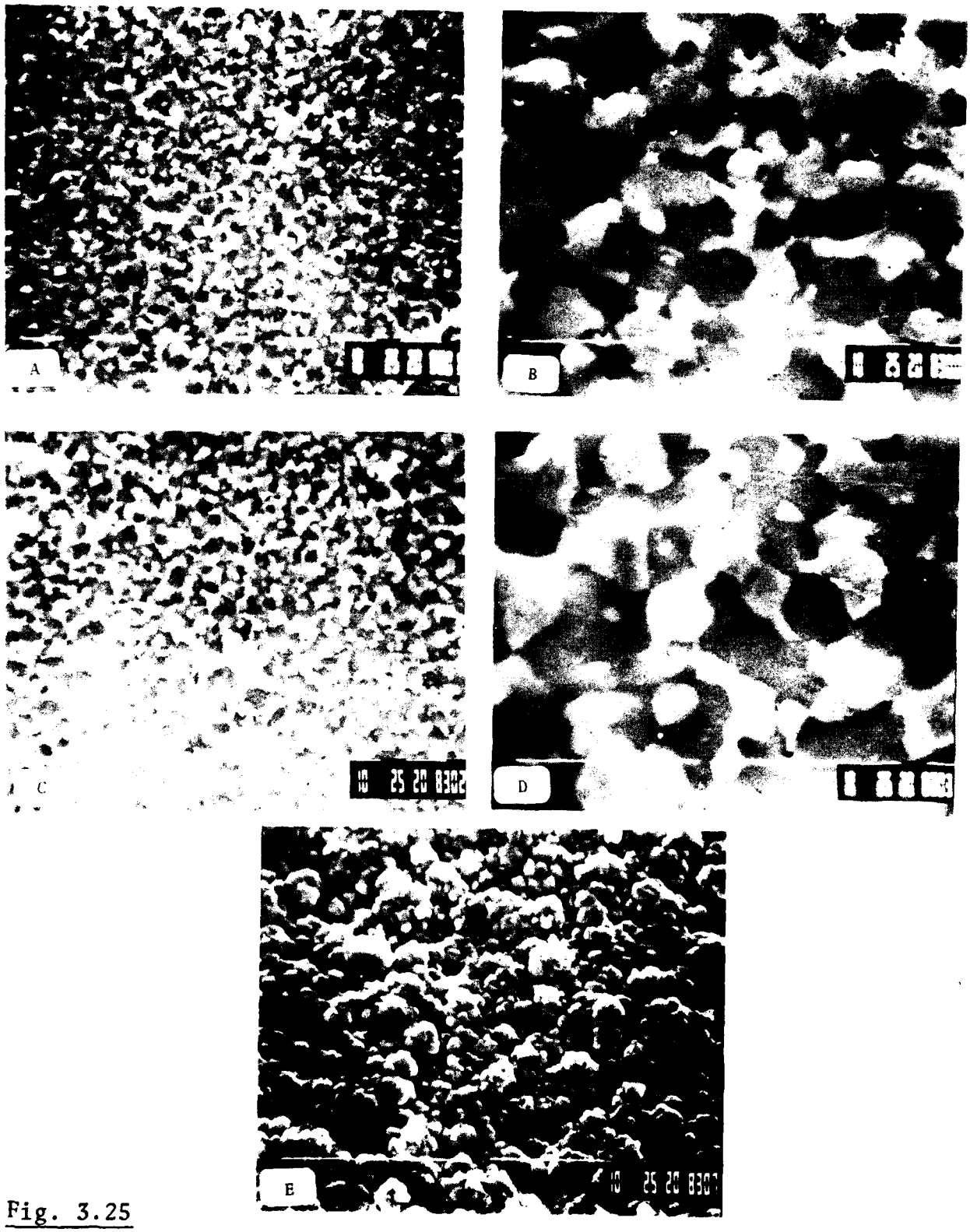

Fig. 3.25

SEM observations of high energy laser treated surface of Pb-Sn coating.

A. Laser treated surface one line x 1000.
B. Higher magnificance of A. x 5000.
C. Two overlapping lines x 1000
D. Higher magnificance of C, x 5000
E. Without laser treatment x 5000.

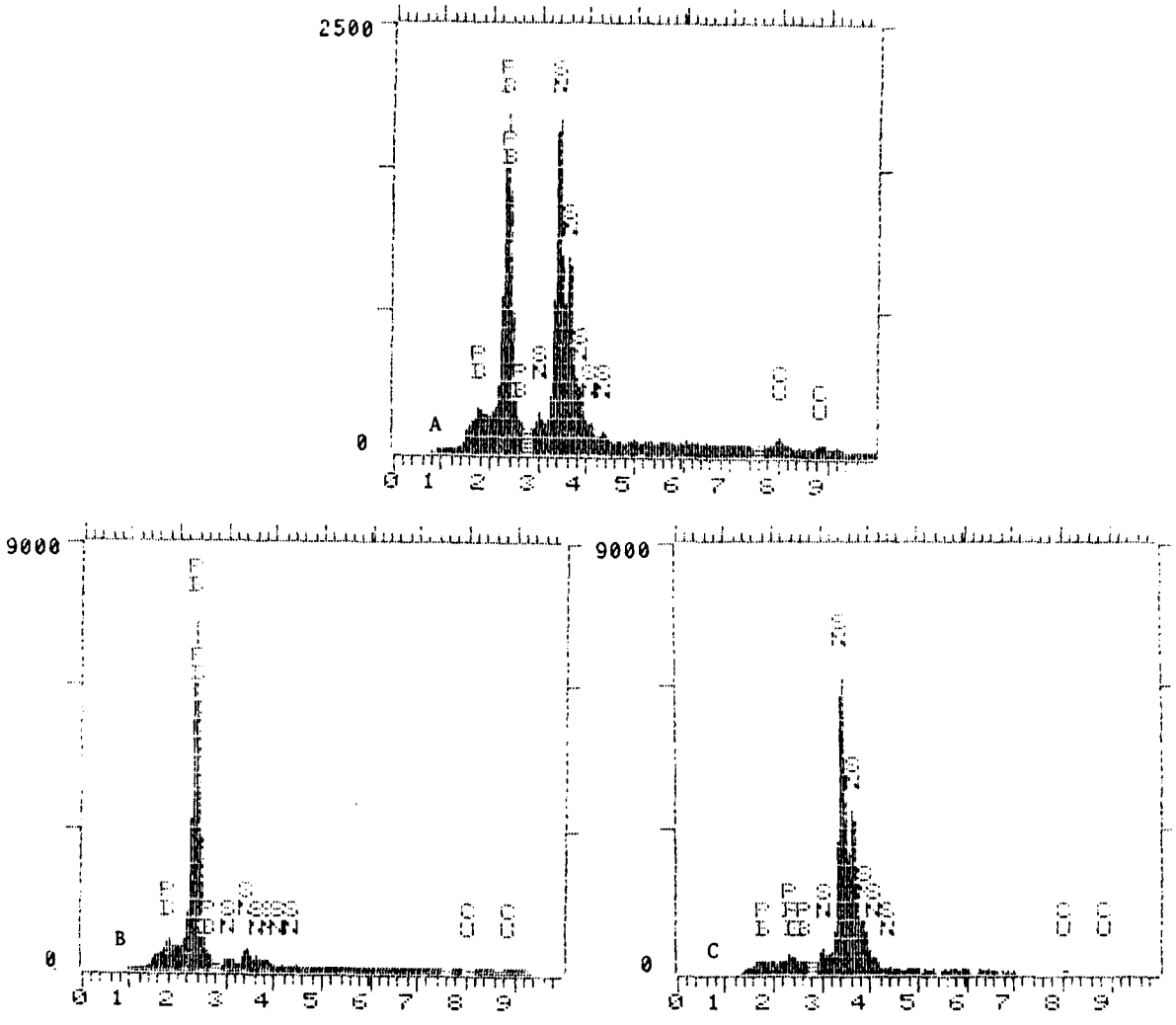

Fig. 3.26 E.D.S analysis of the area shown in Fig. 3.24,
A. Overall area.
B. Bright area
C. Grey area.

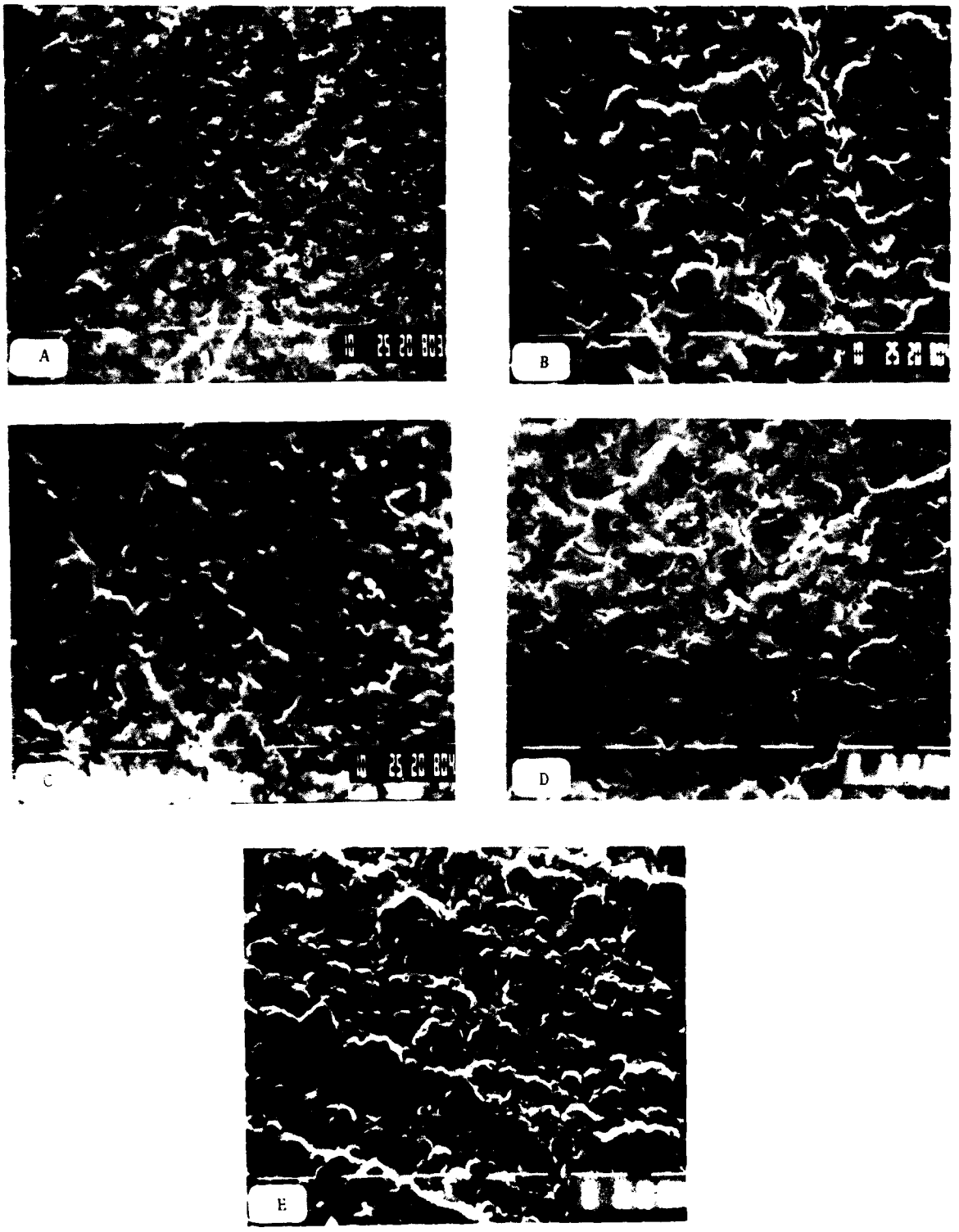

Fig. 3.27: SEM observations of commercial Pb-Sn coating after laser treatment (x 2000). A. Laser energy of 5.10^7 watt/cm^2 B,C. Laser energy of 3.10^7 watt/cm^2. D. Laser energy of $3.8.10^7$ watt/cm^2. E. without laser treatment.

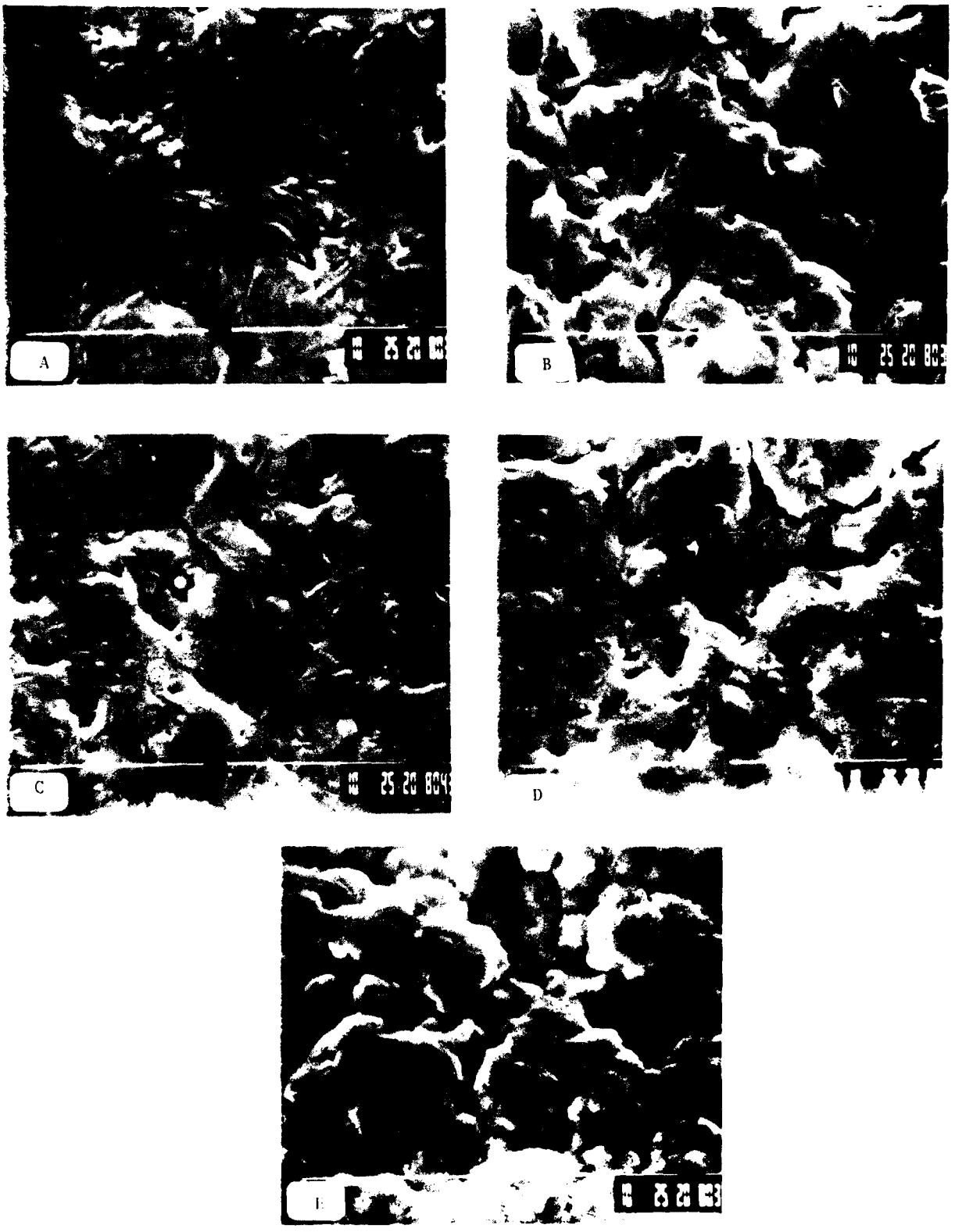

Fig. 3.28:

SEM observations of commercial Pb-Sn specimen.
Fig. 3.27 at higher magnification (x5000). A. Laser energy of 5.10^7 watt/cm^2. B,C. Laser energy of 3.10^7 watt/cm^2.
D. Laser energy of $3.8.10^7$ watt/cm^2. E. Without laser treatment.

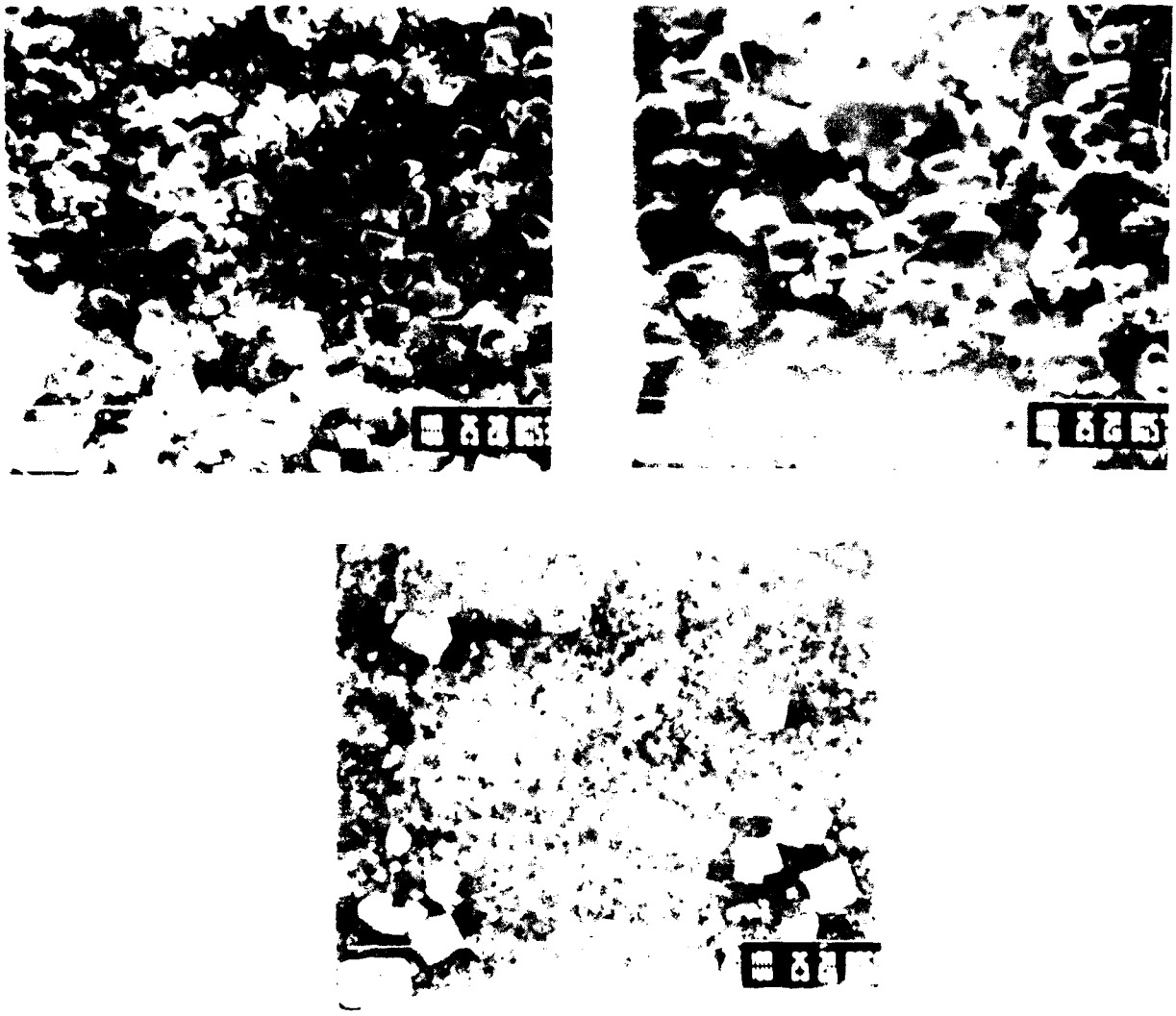

Fig. 3.29 SEM observations of corroded Pb-Sn commercial specimen after polarization in 10^{-2}M NaCl,(x 750).

A. After laser treatment of 5.10^7 watt/cm^2.
B. After laser treatment of 3.10^7 watt/cm^2
C. With laser treatment

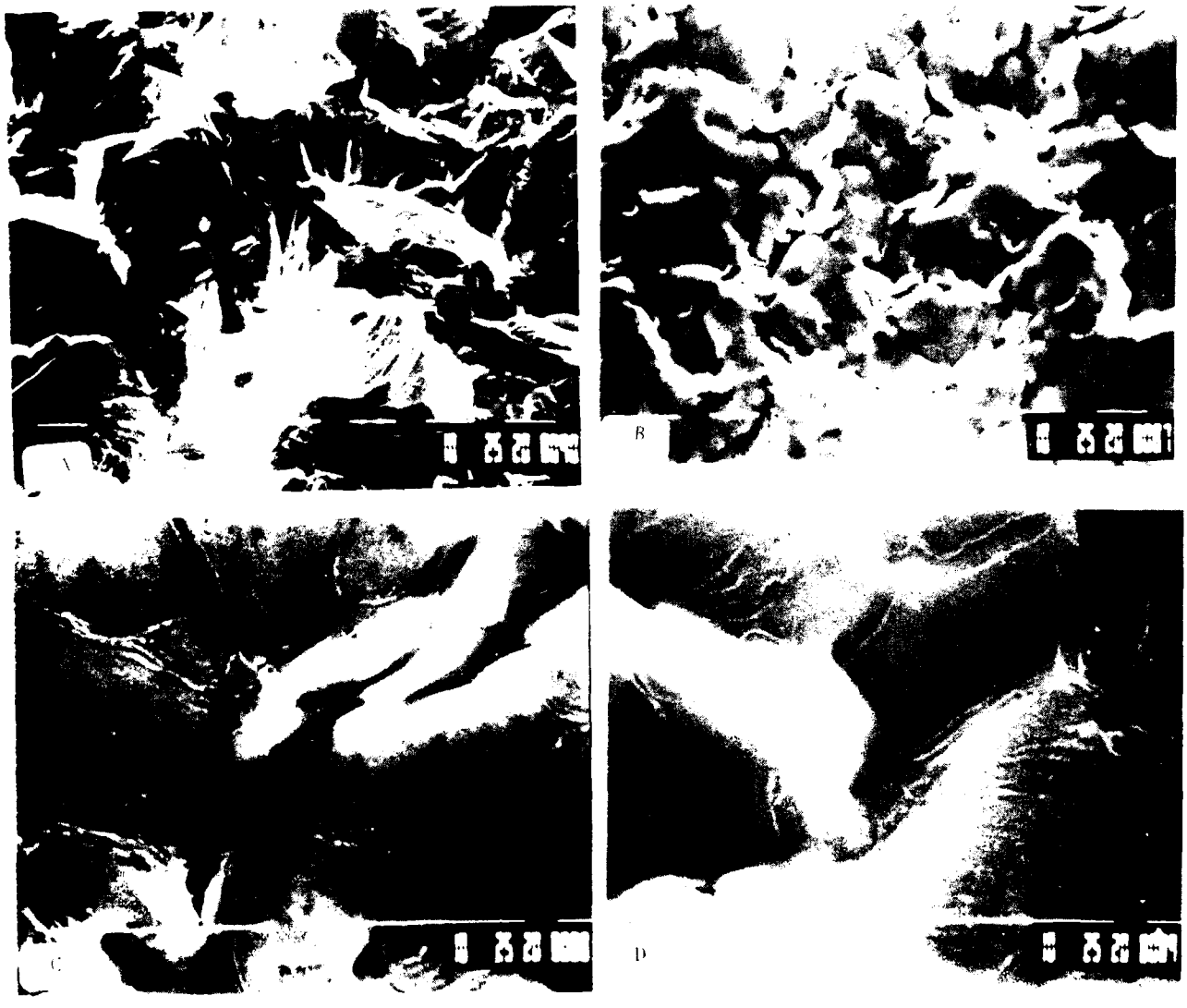

Fig. 3.30 SEM observations of tin surface before and after laser treatment (coating thickness 6.7µm).

A. As deposited x 1000.
B. After laser treatment x 1000
C,D. After laser treatment x 5000

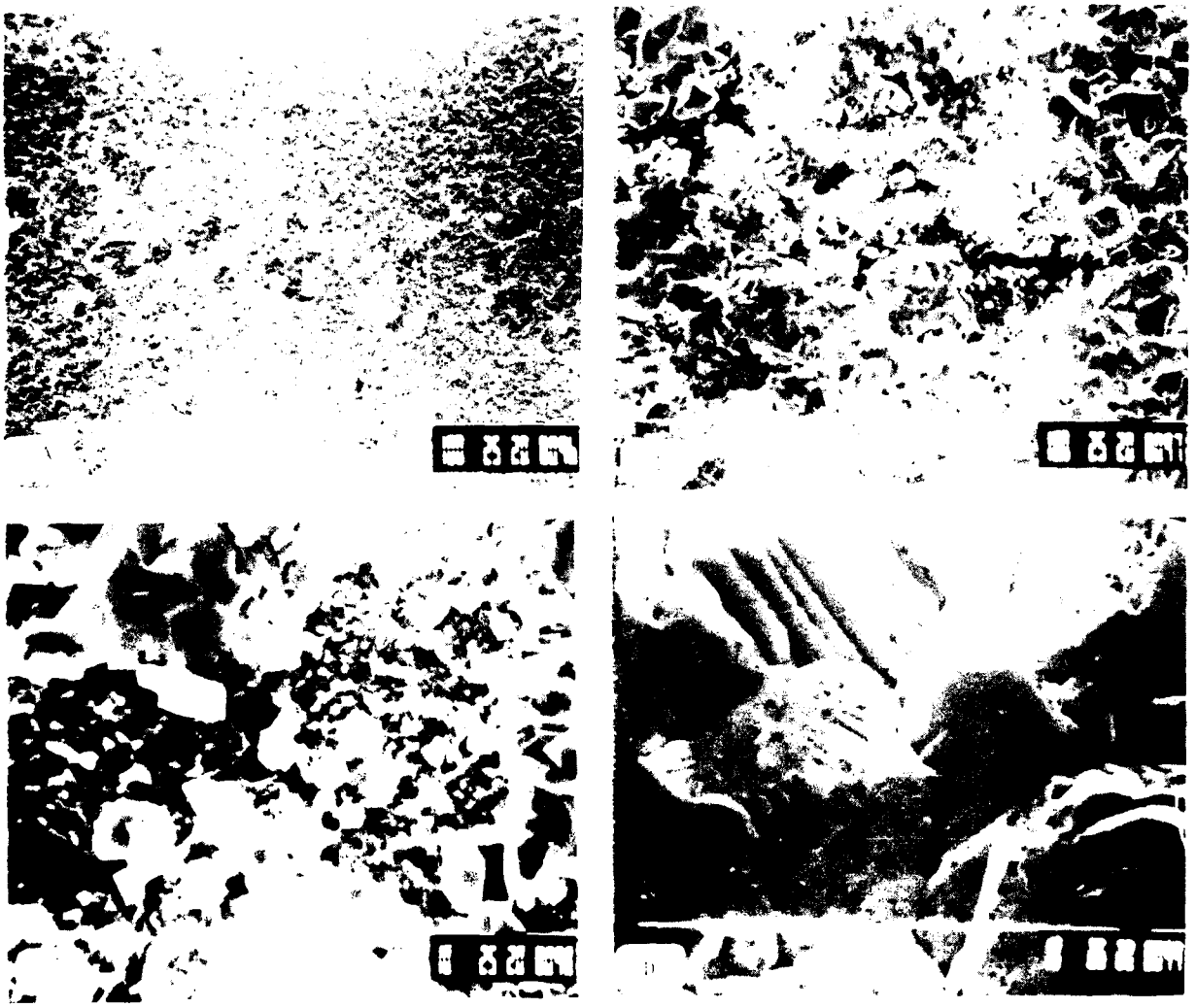

Fig. 3.31 SEM observations of corroded tin specimen after polarization 10^{-2}M NaCl (coating thickness 0.9 µm).
A. Corroded area x 75.
B. Enlargment of the corroded area x 500.
C. Enlargment of the corroded area x 2000.
D. Uncorroded area x 5000.

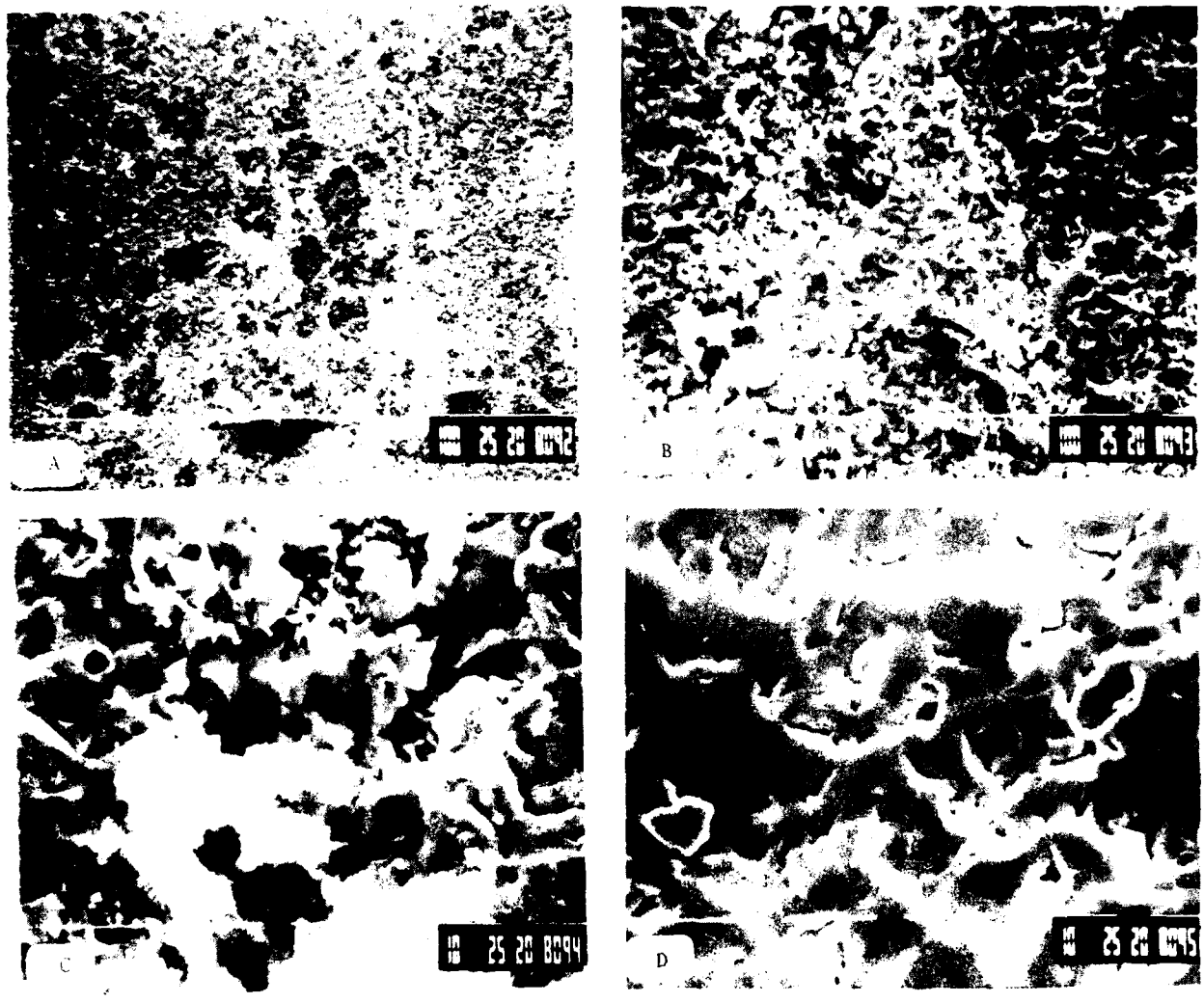

Fig. 3.32 SEM observations of corroded laser treatment tin specimen. (coating thickness 0.96 μm).

A. Corroded area x 75.
B. Enlargment of the corroded area x 500.
C. Enlargment of the corroded area x 2000.
D. Uncorroded area x 2000.

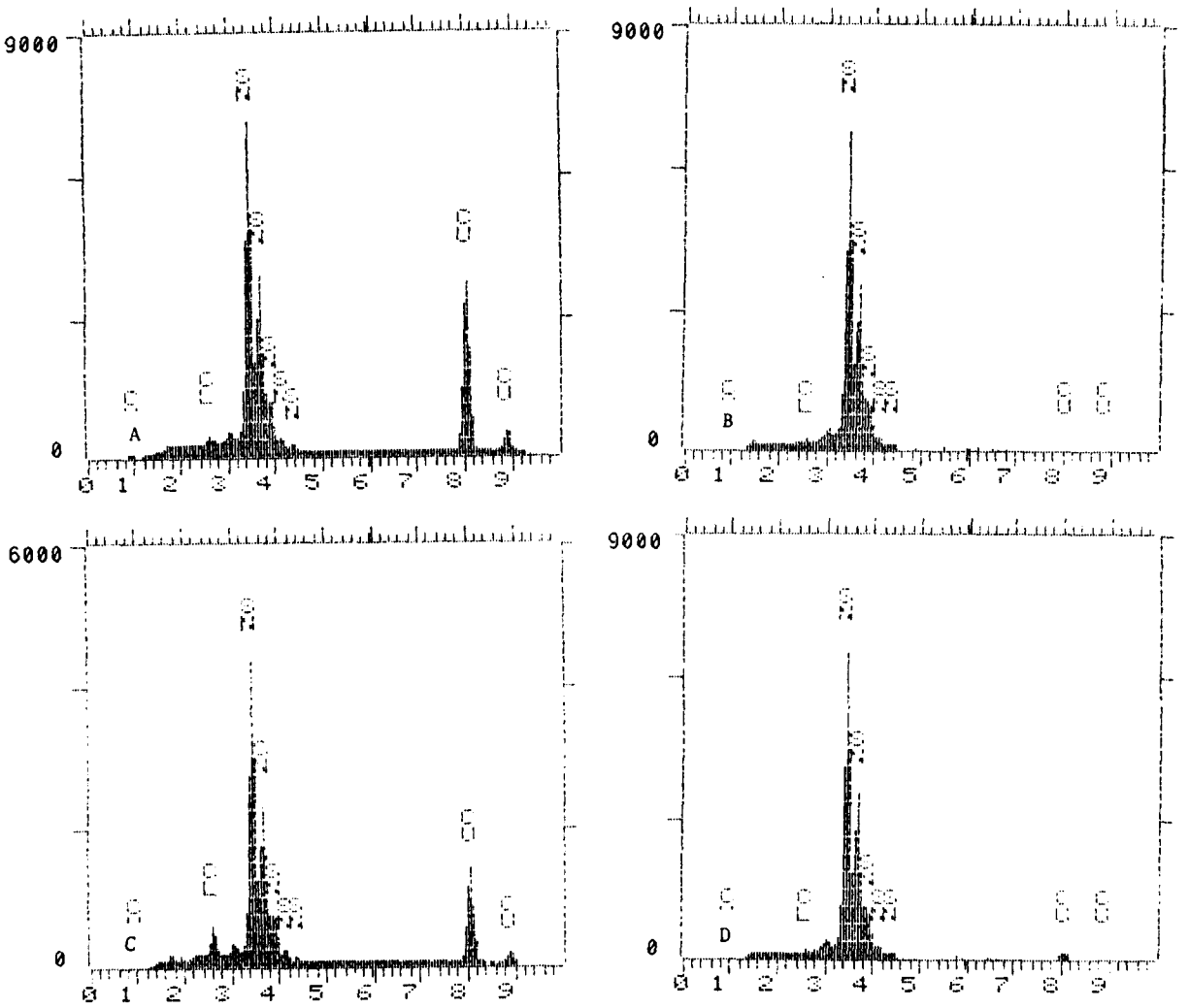

Fig. 3.33 E.D.S analysis of the area shown in Figs. 3.31 ,3.32 .
A. Corroded area without laser treatment (Fig. 3.31)
B. Uncorroded area without laser treatment (Fig. 3.31).
C. Corroded area without laser treatment specimen (Fig. 3.32).
D. Uncorroded area, laser treatment specimen (Fig. 3.32).

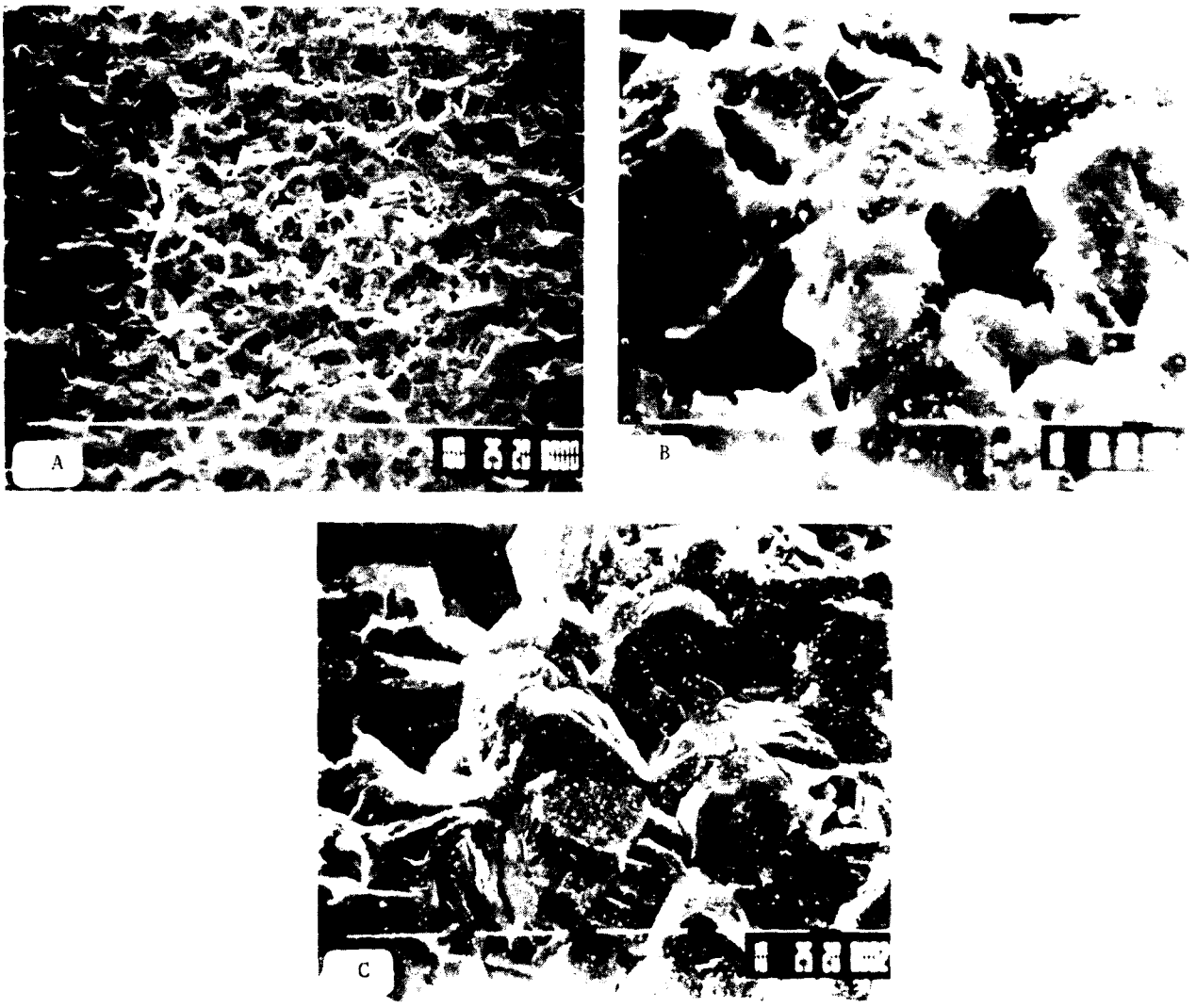

Fig. 3.34 SEM observations of corroded tin area withoutlaser treatment.(Coating thickness 3.6µm).

A. x 500
B. x 5000
C. Uncorroded area x 2000

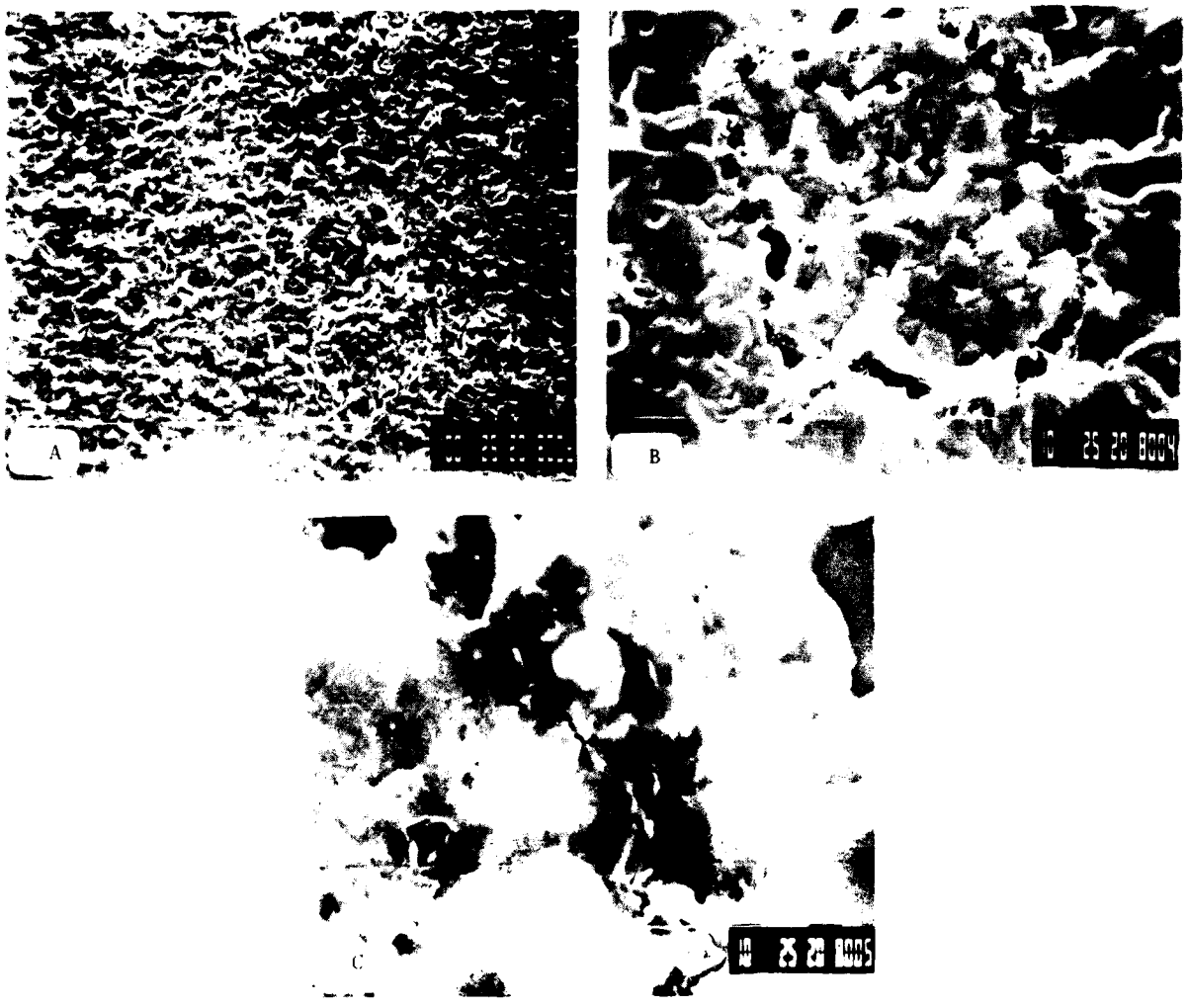

Fig. 3.35 SEM observations of corroded laser treated tin specimen. (Coating thickness 3.6 μm).

A. Corroded area x 200.
B. Enlargment of the corroded area x 2000.
C. x 5000.

END
DATE
FILMED
7-88
DTIC